Is structure based drug design ready for selectivity optimization?

Steven K. Albanese[1,2], John D. Chodera[2], Simon Peng[3], Robert Abel[3], Lingle Wang[3*]

[1]Louis V. Gerstner, Jr. Graduate School of Biomedical Sciences, Memorial Sloan Kettering Cancer Center, New York, NY 10065; [2]Computational and Systems Biology Program, Sloan Kettering Institute, Memorial Sloan Kettering Cancer Center, New York, NY 10065; [3]Schrödinger, New York, NY 10036

***For correspondence:** lingle.wang@schrodinger.com (LW)

Abstract

Alchemical free energy calculations are now widely used to drive or maintain potency in small molecule lead optimization, where the binding affinity to a protein target can be computed—in well-behaved cases—to roughly 1 kcal/mol inaccuracy, which is believed to primarily stem from force field errors. Despite this, the potential to use free energy calculations to drive optimization of compound *selectivity* among two similar targets has been relatively unexplored. In the most optimistic scenario, the similarity of binding sites might lead to a fortuitous cancellation of force field errors and allow selectivity to be predicted more accurately than affinity. Here, we assess the accuracy with which selectivity can be predicted in the context of small molecule kinase inhibitors, considering the very similar binding sites of human kinases CDK2 and CDK9, as well as another series of ligands attempting to achieve selectivity between the more distantly related kinases CDK2 and ERK2. Using a Bayesian analysis approach, we separate force field error from statistical error and quantify the correlation in force field errors between selectivity targets. We find that, in the closely related CDK2/CDK9 case, a high correlation in force field errors suggests free energy calculations can have significant impact in aiding chemists in achieving selectivity, while in more distantly related kinases (CDK2/ERK2), limited correlation in force field errors reduces the ability for free energy calculations to aid selectivity optimization. In both cases, the correlation in force field error suggests that longer simulations are beneficial to properly balance statistical error with systematic error to take full advantage of the increase in accuracy in selectivity prediction possible due to fortuitous cancellation of error.

Free energy methods have proven useful in aiding structure-based drug design by driving the optimization or maintenance of potency in lead optimization. Alchemical free energy calculations allow for prediction of ligand binding free energies, including all enthalpic and entropic contributions [1]. Advances in atomistic molecular mechanics forcefields and free energy methodologies [2–5] have allowed free energy methods to reach a level of accuracy sufficient for predicting ligand potencies [6]. These methods have been applied prospectively to develop inhibitors for Tyk2 [7], Syk [8], BACE1 [9], GPCRs [10], and HIV protease [11]. A recent large-scale review found that the use of FEP+ [12] to predict potency for 92 different projects and 3021 compounds found a median root mean squared error (RMSE) of 1 kcal/mol [13].

Selectivity is an important consideration in drug design

In addition to potency, selectivity is an important property to consider in drug development, either in the pursuit of an inhibitor that is maximally selective [14, 15] or possesses a desired polypharmacology [16–20]. Controlling selectivity can be useful not only in avoiding off-target toxicity (arising from inhibition of unintended targets) [21, 22], but also in avoiding on-target toxicity (arising from inhibition of the intended target) by selectively targeting disease mutations [23]. In either paradigm, considering the selectivity of

a compound is complicated by the biology of the target. For example, kinases exist as nodes in complex signaling networks [24, 25] with feedback inhibition and cross-talk between pathways. Careful consideration of which off-targets are being inhibited can avoid off-target toxicity due to alleviating feedback inhibition and inadvertently reactivating the targeted pathway [24, 25], or the upregulation of a secondary pathway by alleviation of cross-talk inhibition [26, 27]. Off-target toxicity can also be caused by inhibiting unrelated targets, such as gefitinib, an EGFR inhibitor, inhibiting CYP2D6 [21] and causing hepatotoxicity in lung cancer patients. In a cancer setting, on-target toxicity can be avoided by considering the selectivity for the oncogenic mutant form of the kinase over the wild type form of the kinase [28–30], exemplified by number of first generation EGFR inhibitors. Selectivity considerations can also lead to beneficial effects: Imatinib, intially developed to target BCR-Abl fusion proteins, is also approved for treating gastrointestinal stromal tumors (GIST) [31] due to its activity against receptor tyrosine kinase KIT.

Use of physical modeling to predict selectivity is relatively unexplored

While engineering compound selectivity is important for drug discovery, the utility of free energy methods for predicting this property with the aim of reducing the number of compounds that must be synthesized to achieve the desired selectivity has been relatively unexplored. If there is fortuitous cancellation of systematic (forcefield) errors for closely related systems, free energy methods may be much more accurate than expected given the errors made in predicting the potency for each individual target. Molecular dynamics and free energy calculations have been used to extensively study the selectivity of imatinib for Abl kinase over Src [32, 33] and within a family of non-receptor tyrosine kinases [34]. This work focuses on understanding the role reorganization energy plays in the exquisite selectivity of imatinib for Abl over Src despite high similarity between the cocrystallized binding mode and kinase conformations, and does not touch on the evaluation of the accuracy of these methods, or their application to drug discovery on congeneric series of ligands. Previous work predicting the selectivity of three bromodomain inhibitors accross the bromodomain family achieved promising accuracy for single target potencies of roughly 1 kcal/mol, but does not explicitly evaluate any selectivity metrics [35] or look at correlation in the errors made for each bromodomain.

Kinases are an interesting and particularly challenging model system for selectivity predictions

Kinases are a useful model system to work with for assessing the utility of free energy calculations to predict inhibitor selectivity in a drug discovery context. With the approval of imatinib for the treatment of chronic myelogenous leukemia in 2001, targeted small molecule kinase inhibitors (SMKIs) have become a major class of therapeutics in treating cancer and other diseases. Currently, there are 43 FDA-approved SMKIs [36], and it is estimated that kinase targeted therapies account for as much as 50% of current drug development [37], with many more compounds currently in clinical trials. While there have been a number of successes, the current stable of FDA-approved kinase inhibitors targets only a small number of kinases implicated in disease, and the design of new selective kinase inhibitors remains a significant challenge.

Achieving selective inhibition of kinases is quite challenging, as there are more than 518 protein kinases [38, 39] sharing a highly conserved ATP binding site that is targeted by the majority of SMKIs [40]. While kinase inhibitors have been designed to target kinase-specific subpockets and binding modes to achieve selectivity [41–46], previous work has shown that both Type I (binding to the active, DFG-in conformation) and Type II (binding to the inactive, DFG-out conformation) inhibitors display a range of selectivities [47, 48], often exhibiting significant binding to a number of other targets in addition to their primary target. Even FDA-approved inhibitors—often the result of extensive drug development programs—bind to a large number of off-target kinases [49]. Kinases are also targets of interest for developing polypharmacological compounds, or inhibitors that are specifically designed to inhibit multiple kinase targets. Resistance to MEK inhibitors in KRAS-mutant lung and colon cancer has been shown to be driven by HER3 upregulation [50], providing a rationale for dual MEK/ERBB family inhibitors. Similarly, combined MEK and VEGFR1 inhibition has been proposed as a combinatorial approach to treat KRAS-mutant lung cancer [51]. Developing inhibitors with the desired polypharmacology means navigating more complex selectivity profiles, presenting a problem where physical modeling has the potential to dramatically speed up drug discovery.

Assessing the ability of alchemical free energy methods to predict selectivity

Since the prediction of selectivity depends on predicting affinities to two or more targets (or relative affinities between pairs of related molecules), a spectrum of possibilities exists for the accuracy of predicted selectivity metrics. In well-behaved kinase systems, for example, free energy calculation potency predictions have achieved mean unsigned errors of less than 1.0 kcal/mol [7, 12], believed to arise predominantly from systematic force field errors [4]. In the best-case scenario, the force field errors for two protein targets might exactly cancel out, allowing selectivity to be predicted more accurately than potency; on the other hand, if the force field error acts like a random error between two distinct (but potentially related) protein targets, predictions of selectivity will be *less accurate* than potency predictions. Real-world systems are likely to be somewhere between these extremes, and quantifying the *degree* to which error in multiple protein targets is correlated, its implications for the use of free energy calculations for prioritizing synthesis in the pursuit of selectivity, the ramifications for optimal calculation protocols, and rough guidelines governing which systems we might expect good selectivity prediction is the primary focus of this work.

Here, we investigate the magnitude of the correlation (ρ) in predicted binding free energy differences between compounds to two different targets ($\Delta\Delta G$), assessing the utility of alchemical free energy calculations for the prediction of selectivity. We employ state of the art relative free energy calculations [12, 13] to predict the selectivities of two different congeneric ligand series [52, 53], as well as present simple numerical models to quantify the potential speed up in selectivity optimization expected for different combinations of per target forcefield errors and correlation coefficient values. To tease out the effects of a limited number of experimental measurements, we develop a new Bayesian approach to quantify the uncertainty in the correlation coefficient in the predicted change in selectivity on ligand modification, incorporating all sources of uncertainty and correlation in the computation to separate statistical from force field error. We find that in the closely related systems of CDK2 and CDK9, a high correlation of force field errors suggests that free energy methods can have a significant impact on speeding up selectivity optimization. Even in the more distantly related case (CDK2/ERK2), correlation in the forcefield errors allows free energy calculations to speed up selectivity optimization, suggesting that these methodologies can impact drug discovery even when comparing systems that are not closely related. We present a model of the impact of per target statistical error at different levels of forcefield error correlation, suggesting that it is worthwhile to expend more effort sampling in systems with high correlation.

Results

Free energy methods can be used to predict the selectivity of a compound

While ligand potency for a single target is often quantified as a free energy of binding ($\Delta G_{\text{binding}}$), there are a number of different metrics for quantifying the selectivity of a compound [54, 55]. Here, we propose a more granular view of selectivity: the change in free energy of binding for a given ligand between two different targets ($\Delta\Delta G_{\text{selectivity}}$), which can be calculated as in Equation 1. $\Delta\Delta G_{\text{selectivity}}$ is a useful measure of compound selectivity once a single, or small panel, of off-targets have been identified.

$$\Delta\Delta G_{\text{selectivity}} = \Delta G_{\text{binding, target 2}} - \Delta G_{\text{binding, target 1}} \tag{1}$$

To predict the $\Delta\Delta G_{\text{selectivity}}$ of a compound, we developed a protocol that uses a relative free energy calculation (FEP+) [12] to run a map of perturbations between ligands in a congeneric series, as described in depth in the methods section. The calculation is repeated for each target of interest, with identical perturbations (edges) between each ligand (nodes). Each edge represents a relative free energy calculation that quantifies the $\Delta\Delta G$ between the ligands, or nodes. By using provided experimental data, we can convert the $\Delta\Delta G$ from each edge to a single potency value for each value against that target (ΔG_{target}). From this sets of calculations, we can calculate a $\Delta\Delta G_{selectivity}$ for each ligand given two targets of interest. Previous work shows that FEP+ can achieve an accuracy (σ_{target}) of roughly 1 kcal/mol when predicting potency, which is a combination of systematic forcefield and random statistical error [12]. However, it is possible that the forcefield component of that error (σ_{ff}) may fortuitously cancel when computing $\Delta\Delta G_{selectivity}$, leading to a forcefield component of the selectivity uncertainty that is lower than would be expected.

Correlation of errors can make selectivity predictions more accurate and speed up ligand optimization

To demonstrate the potential impact correlation has on the forcefield error of selectivity predictions ($\sigma_{selectivity}$) using alchemical free energy techniques, we created a simple numerical model following Equation 2, which takes into account each of the per target forcefield errors expected from the methodology as well as the correlation in those errors. As seen in Figure 1A, if the per target forcefield errors ($\sigma_{ff,1}$ and $\sigma_{ff,2}$) are the same, $\sigma_{selectivity}$ approaches 0 as the correlation coefficient (ρ) approaches 1. If the error for the free energy method is not the same, $\sigma_{selectivity}$ gets smaller but approaches a non-zero value as ρ approaches 1. To quantify the expected speedup in selectivity optimization, we modeled the change in selectivity with respect to a reference compound for a number of compounds a medicinal chemist might suggest as a normal distribution centered around 0 with a standard deviation of 1 kcal/mol (Figure 1B, black curve), reflecting that most proposed modifications would not drive large changes in selectivity. Then, suppose that each compound is screened computationally with a free energy methodology with a per target forcefield error (σ_{ff}) of 1 kcal/mol in the regime of infinite computational effort where statistical error is 0 kcal/mol. All compounds predicted to have a 1.4 kcal/mol improvement in selectivity are synthesized and experimentally tested (Figure 1B, colored curves), using an experimental technique with perfect accuracy. The fold-change in the proportion of compounds that are made that have a true 1.4 kcal/mol improvement in selectivity compared to the original distribution can be calculated as a surrogate for the expected speedup. For a 1.4 kcal/mol selectivity improvement threshold (1 log unit), a correlation of 0.5 gives an expected speed up of 4.1x, which can be interpreted as need to make 4.1x fewer compounds to achieve a 1 log unit improvement in selectivity. This process can be extended for the even more difficult proposition of achieving a 2 log unit improvement in selectivity (Figure 1C), where 200–300× speedups can be expected, depending on σ_{ff} for the free energy methodology.

The CDK2 and CDK9 experimental dataset demonstrates the difficulty in achieving selectivity for closely related kinases.

SKA: I will insert some sentences about the relatedness of the kinases based on Andrea's Volkamer's analysis.

To assess the correlation of errors in free energy predictions for selectivity, we set out to gather datasets that met a number of criteria. We searched for datasets that contained binding affinity data for a number of kinase targets and ligands, as well as having crystal structures for each target with the same co-crystallized ligand. For the CDK2/CDK9 datatset [52], ligand 12c was cocrystallized with CDK2/cylin A (Figure 2A, left) and CDK9/cyclin T (Figure 2B, left), work that was published in a companion paper [56]. In both CDK2 and CDK9, ligand 12c forms relatively few hydrogen bond interactions with the kinase. Each kinase forms a set of hydrogen bonds between the ligand scaffold and a hinge residue (C106 in CDK9 and L83 in CDK2) that is conserved across all of the ligands in this series. CDK9, which has slightly lower affinity for ligand 12c (Figure 2C, right), forms a lone interaction between the sulfonamide of ligand 12c and residue E107. On the other hand, CDK2 forms interactions between the sulfonamide of ligand 12c and residues K89 and H84. The congeneric series of ligands contains a number of challenging perturbations, particularly at substituent point R3 (Figure 2C, left). Ligand 12i also presented a challenging perturbation, moving the 1-(piperazine-1-yl)ethanone from the *meta* to *para* location.

This congeneric series of ligands also highlights two of the challenges of working from publicly available data. First, the dynamic range of selectivity is incredibly narrow, with a mean $\Delta\Delta G_{selectivity}$ (CDK9 - CDK2) of only -0.65 kcal/mol, and a standard deviation of 0.88 kcal/mol. The total dynamic range of this dataset is 2.8 kcal/mol.

Additionally, experimental uncertainties are not reported for the experimental measurements. Thus, for this and subsequent sets of ligands, the experimental uncertainty is assumed to be 0.3 kcal/mol based on previous work done to summarize uncertainty in experimental data [6, 57].

The CDK2 and ERK2 dataset achieves higher levels of selectivity for more distantly related kinases

The CDK2/ERK2 datatset from Blake et al. [53] also met the criteria described above. Crystal structures for both CDK2 (Figure 3A, top) and ERK2 (Figure 3B, top) were available with ligand 22 co-crystallized. Of note, CDK2 was not crystallized with cyclin A, despite cyclin A being included in the affinity assay reported in the

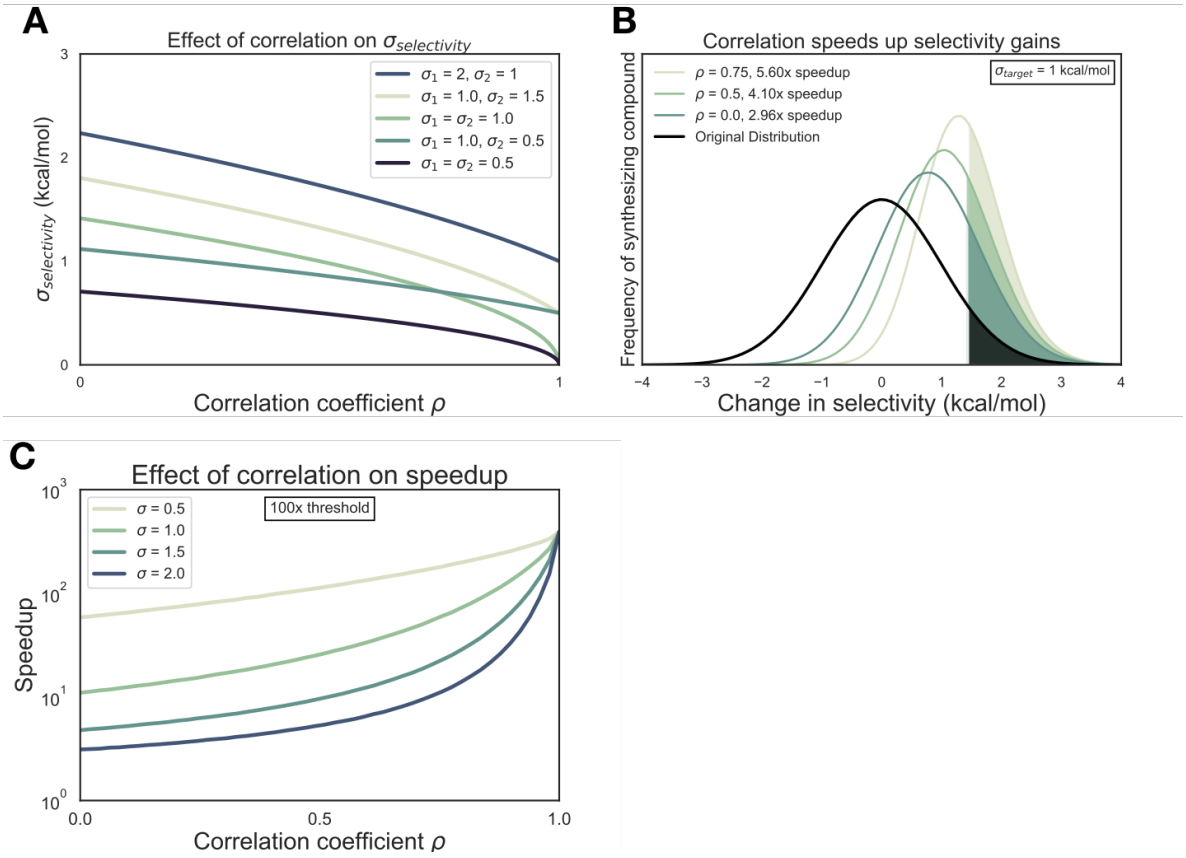

Figure 1. Free energy calculations can accelerate selectivity optimization. (**A**) The effect of correlation on expected errors for predicting selectivity ($\sigma_{selectivity}$) in kcal/mol. Each curve represents a different combination of per target forcefield errors ($\sigma_{ff,1}$ and $\sigma_{ff,2}$). (**B**) The change in selectivity for molecules proposed by medicinal chemists optimizing a lead candidate can be modeled by a normal distribution centered on zero with a standard deviation of 1 kcal/mol (black curve), which is consistent with the standard deviation of selectivities observed in the experimental data presented later in this work. Each green curve corresponds to the distribution of compounds made after screening for a 1 $\log_{10}$ unit (1.4 kcal/mol) improvement in selectivity with a free energy methodology with a 1 kcal/mol per target forcefield error and a particular correlation, in the regime of infinite error where statistical error is zero. The shaded region of each curve corresponds to the compounds with a real 1 $\log_{10}$ unit improvement in selectivity. The speedup is calculated as the ratio of the percentage of compounds made with a real 1 $\log_{10}$ unit improvement to the percentage of compounds that would be expected in the original distribution. (**C**) The speedup (y-axis, log scale) expected for 100× (2 $\log_{10}$ units, or 2.8 kcal/mol) selectivity optimization as a function of correlation coefficient ρ. Each curve corresponds to a different value of σ_{ff}.

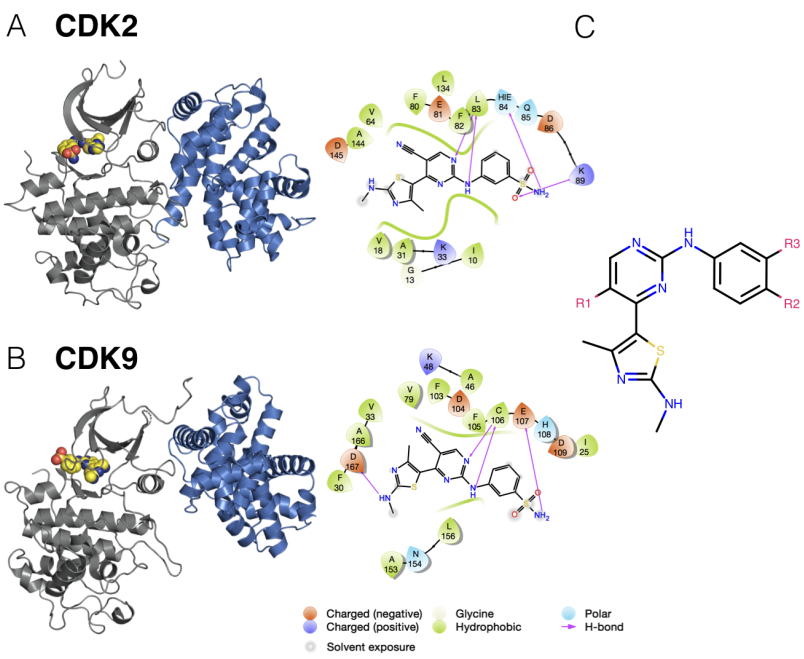

Ligand	R1	R2	R3	ΔG CDK2 (kcal/mol)	ΔG CDK9 (kcal/mol)	ΔΔG (kcal/mol)
12a	CN	H		-12.27	-11.21	1.06
12b	OH	H		-7.23	-8.22	-0.99
12c	CN	H		-11.45	-11.21	0.24
12e	F	H		-11.62	-11.45	0.17
12f	Cl	H		-10.91	-10.85	0.06
12g	Methyl	H		-10.18	-11.32	-1.14
12h	Ethyl	H		-8.28	-9.56	-1.28
12j	CN	H		-10.04	-11.12	-1.08
12l	CN		H	-10.34	-10.44	-0.1
12n	CN	H		-10.06	-10.97	-0.91
12o	F	H		-10.06	-11.12	-1.06
12q	F	H		-10.91	-11.62	-0.71
12t	CN	H		-9.38	-11.12	-1.74
1a	H	H		-11.62	-11.86	-0.24
1b	H	H		-11.45	-11.86	-0.41

Figure 2. A CDK2/CDK9 selectivity dataset. Experimental IC_{50} data for a congeneric series of compounds binding to CDK2 and CDK9 was extracted from Shao et al. [52]. (**A**) *(left)* Crystal Structure (4BCK)[56] of CDK2 (gray ribbon) bound to ligand 12c (yellow spheres). Cyclin A is shown in blue ribbon. *(right)* 2D ligand interaction map of ligand 12c in the CDK2 binding site. (**B**) *(left)* Crystal structure of CDK9 (4BCI)[56] (gray ribbon) bound to ligand 12c (yellow spheres). Cyclin T is shown in blue ribbon. *(right)* 2D ligand interaction map of ligand 12c in the CDK9 binding site. (**C**) *(left)* 2D structure of the common scaffold for all ligands in congeneric ligand series 12 from the publication. *(right)* A table summarizing all R group substitutions as well as the published experimental binding affinities and selectivities [52].

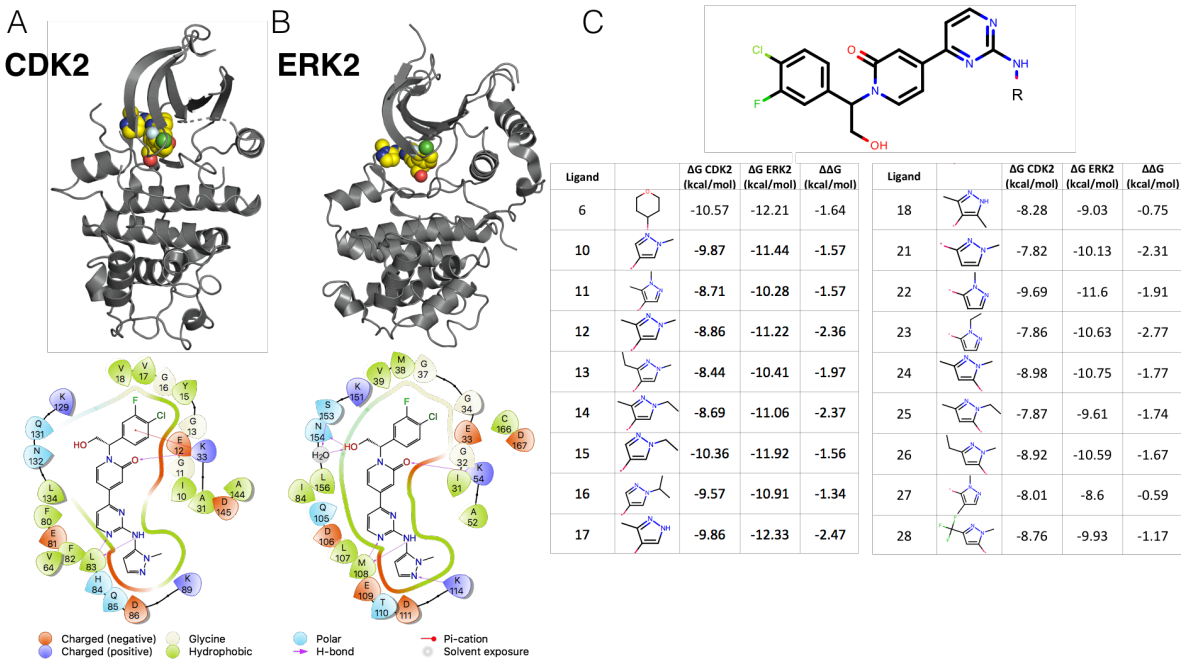

Ligand		ΔG CDK2 (kcal/mol)	ΔG ERK2 (kcal/mol)	ΔΔG (kcal/mol)
6		-10.57	-12.21	-1.64
10		-9.87	-11.44	-1.57
11		-8.71	-10.28	-1.57
12		-8.86	-11.22	-2.36
13		-8.44	-10.41	-1.97
14		-8.69	-11.06	-2.37
15		-10.36	-11.92	-1.56
16		-9.57	-10.91	-1.34
17		-9.86	-12.33	-2.47

Ligand		ΔG CDK2 (kcal/mol)	ΔG ERK2 (kcal/mol)	ΔΔG (kcal/mol)
18		-8.28	-9.03	-0.75
21		-7.82	-10.13	-2.31
22		-9.69	-11.6	-1.91
23		-7.86	-10.63	-2.77
24		-8.98	-10.75	-1.77
25		-7.87	-9.61	-1.74
26		-8.92	-10.59	-1.67
27		-8.01	-8.6	-0.59
28		-8.76	-9.93	-1.17

Figure 3. CDK2 and ERK2 selectivity dataset from Blake et *al*., 2016
(**A**) *(top)* Crystal structure of CDK2 (5K4J) shown in gray cartoon and ligand 22 shown in yellow spheres. *(bot)* 2D interaction map of ligand 22 in the binding pocket of CDK2 (**B**) *(top)* Crystal structure of ERK2 (5K4I) shown in gray cartoon with ligand 22 shown in yellow spheres. *(bot)* 2D interaction map of ligand 22 in the binding pocket of ERK2. (**C**) *(top)* Common scaffold for all of the ligands in the Blake dataset, with R denoting attachment side for substitutions. *(bot)* Table showing R group substitutions and experimentally measured binding affinities and selectivities. Ligand numbers correspond to those used in publication.

paper [53]. CDK2 adopts a DFG-in conformation with the αC helix rotated out, away from the ATP binding site and breaking the conserved salt bridge between K33 and E51 (Supplementary Figure 1A), indicative of an inactive kinase [43, 58]. By comparison, the CDK2 structure from the CDK2/CDK9 dataset adopts a DFG-in conformation with the αC helix rotated in, forming the ionic bond between K33 and E51 indicative of an active kinase, due to allosteric activation by cyclin A. While missing cyclins have caused problems for free energy calculations in prior work

SKA:is there a good citation for this?

, it is possible that the fully active conformation contributes equally to binding affinity for all of the ligands in the series, and the high accuracy of the potency predictions (Figure 4, top left) is the result of fortutious cancellation of errors.

The binding mode for this series is similar between both kinases. There is a set of conserved hydrogens bonds between the scaffold of the ligand and the backbone of one of the hinge residues (L83 for CDK2 and M108 for ERK2). The conserved lysine (K33 for CDK2 and K54 for ERK2), normally involved in the formation of a ionic bond with the αC helix, forms a hydrogen bond with the scaffold (Figure 4A and 4B, bottom) in both CDK2 and ERK2. However, in the ERK2 structure, the hydroxyl engages a crystallographic water as well as N154 in a hydrogen bond network that is not present in the CDK2 structure. The congeneric ligand series features a single solvent-exposed substituent. This helps explain the extremely narrow distribution of selectivities, with a mean selectivity of -1.74 kcal/mol (ERK2 - CDK2) and standard deviation of 0.56 kcal/mol. The total dynamic range of this dataset is 2.2 kcal/mol. This suggests that the selectivity is largely driven by the scaffold and unaffected by the R-group substitutions.

FEP+ calculations show accurate potency predictions for ERK2/CDK2 and larger errors for CDK2/CDK9

The FEP+ predictions of single target potencies (ΔG) showed good accuracy for the CDK2 and ERK2 dataset (Figure 4, top). Replicate 1 of the calculations is shown in Figure 4, with an RMSE of $0.41^{0.71}_{0.13}$ and $0.79^{1.48}_{0.09}$ kcal/mol, respectively. All of the CDK2 potencies were predicted within 1 log unit of the experimental value, while ERK2 had two outliers. The selectivity ($\Delta\Delta G_{selectivity}$) predictions show an RMSE of $0.77^{1.38}_{0.22}$ kcal/mol, with all but one of the predictions falling within 1 log unit of the experimental values (Figure 4, top right panel). This was consistent across all three replicates of the calculations (Supp. Figure 6). This consistency across replicates holds true at the individual ligand level as well (Supp. Figure 8). Despite the low RMSE for the selectivity predictions, the narrow dynamic range and high uncertainty from experiment and calculation makes it difficult to determine which compounds are more selective than others.

Replicate 1 of the CDK2/CDK9 calculations are shown in the bottom panel of Figure 4. The CDK2 and CDK9 datasets show higher errors in the potency predictions, with an RMSE of $1.04^{1.86}_{0.27}$ and $1.79^{2.65}_{0.84}$ kcal/mol respectively. There are a number of outliers that fall outside of 1 log unit from the experimental value for CDK2 and CDK9. While the higher per target errors make predicting potency more difficult, the selectivity predictions show a much lower RMSE of $0.70^{1.06}_{0.30}$ kcal/mol. This suggests that some correlation in the error is leading to fortuitous cancellation of the forcefield error, leading to more accurate than expected predictions of $\Delta\Delta G_{selectivity}$. These results were consistent across all three replicates of the calculation (Supp. Figure 4) as well as each individual ligand (Supp. Figure 8).

Correlation of forcefield errors accelerates selectivity optimization

To quantify the correlation coefficient (ρ) of the forcefield errors in our calculations, we built a Bayesian graphical model to separate the forcefield error from the statistical error, as described in depth in the methods section. Briefly, we modeled the absolute free energy (G) of each ligand in each phase (complex and solvent) as in equation 8. The model was chained to the FEP+ calculations by providing the $\Delta G^{calc}_{phase,ij,target}$ as observed data, as in equation 10. As in equation, the experimental data was modeled as a normal distribution centered around the true free energy of binding ($\Delta G^{true}_{i,target}$) corrupted by experimental error, which is assumed to be 0.3 kcal/mol from previous work done to quantify the uncertainty in publicly available data [6]. The reported IC50 values from each dataset were treated as data observations (Equation 13) and the $\Delta G^{true}_{i,target}$ was assigned a weak normal prior (Equation 14). The correlation coefficient was calculated for each sample according to equation 15. The correlation coefficient ρ for replicate 1 of the CDK2/ERK2 calculations was quantified to be $0.49^{0.68}_{0.27}$, indicating that the errors are correlated between ERK2 and CDK2 (Figure 6A, right), which was consistent with the distributions for ρ in replicates 2 and 3 (Supp. Figure 7). The joint marginal distribution of the error (ϵ) for each target is more diagonal than symmetric, which is expected for cases in which ρ is 0.5 (Supp. Figure 2). In addition to correlation in the forcefield errors, the high per target accuracy of these calculations allow for a predicted 2-3x speed up for 1 log unit selectivity optimization, and a 20-50x speed up for 2 log unit selectivity optimization (Figure 6A, right), in the regime of infinite sampling effort where there is no statistical error.

The CDK2/CDK9 calculations show strong evidence of correlation, with a correlation coefficient of $0.72^{0.83}_{0.58}$ (Figure 6B, right) for replicate 1. The rest of the replicates showed strong agreement (Supp. Figure 5). The joint marginal distribution of errors is strongly diagonal, which is expected based on the value for ρ (Figure 6B, left). The high correlation in errors leads to a speed up of 2-3 for 1 log unit selectivity optimization and 30-40x for 2 log unit selectivity optimization (Figure 6B, right), despite the much higher per target RMSE than the CDK2/ERK2 case.

Quantifying ρ for these calculations enables estimation of the forcefield error in the selectivity predictions, $\sigma_{selectivity}$. This is useful for estimating expected error for prospective studies, where the experimental values for $\Delta\Delta G_{selectivity}$ are not yet known. Based on the distribution quantified for ρ, the expected $\sigma_{selectivity}$ for the CDK2/CDK9 calculations is $1.18^{1.38}_{0.95}$ kcal/mol (Supp. Figure 3), which is in good agreement with the bootstrapped RMSE (Figure 4, bottom). For the CDK2/ERK2 calculations, $\sigma_{selectivity}$ is $0.96^{1.14}_{0.75}$ (Supp. Figure 3), which is also in good agreement with the bootstrapped RMSE (Figure 4, top).

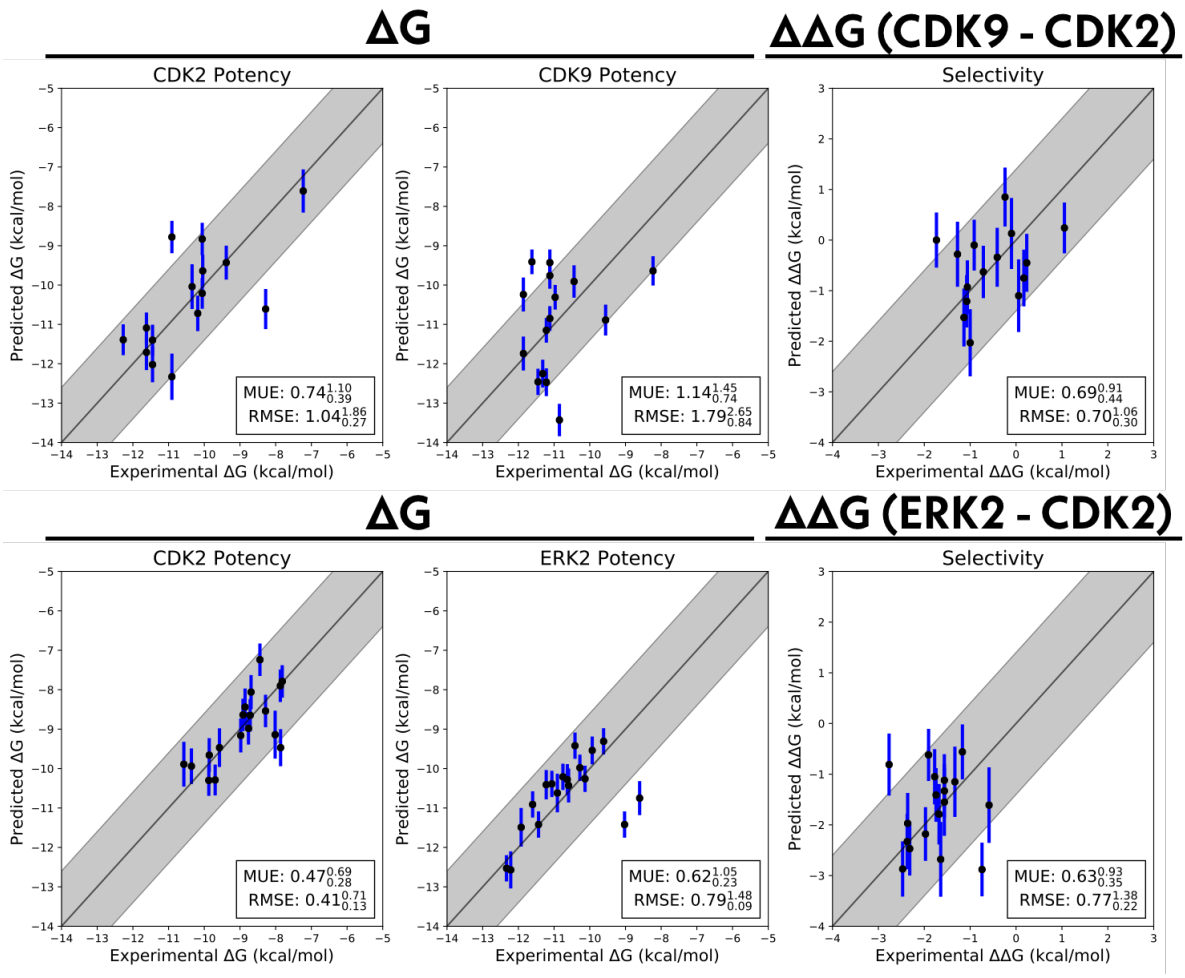

Figure 4. Relative free energy calculations can accurately predict potency, but show larger errors for selectivity predictions.
Single target potencies and selectivities for CDK2/ERK2 from the Blake datasets (*top*), and CDK2/CDK9 (*bottom*) from the Shao datasets. The experimental values are shown on the X-axis and calculated values on the Y-axis. Each data point corresponds to a ligand for a given target. All values are shown in units of kcal/mol. The horizontal error bars show the assumed experimental uncertainty of 0.3 kcal/mol[6]. We show the 95% CI based on the estimated statistical (σ_{stat}) as vertical blue error bars. For selectivity, the errors were propagated under the assumption that they were completely uncorrelated. The black line indicates agreement between calculation and experiment, while the gray shaded region represent 1.36 kcal/mol (or 1 log unit) error. The MUE and RMSE are shown on each plot with bootstrapped 95% confidence intervals.

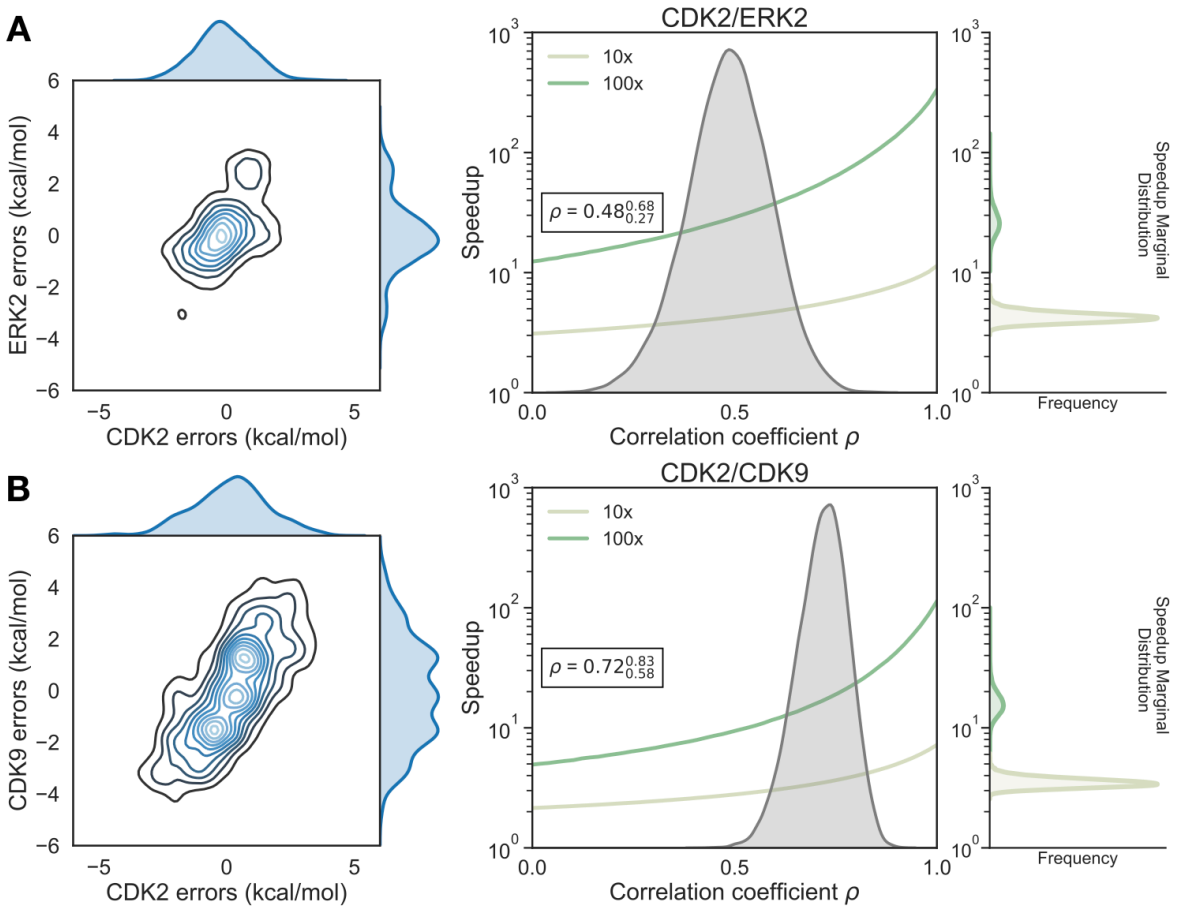

Figure 5. Correlation in force field errors between targets can significantly accelerate selectivity optimization. (**A**, *left*) The joint posterior distribution of the prediction errors for the more distantly related CDK2 (x-axis) and ERK2 (y-axis) from the Bayesian graphical model. (**A**, *right*) Speedup in selectivity optimization (x-axis) as a function of correlation coefficient (x-axis). The posterior marginal distribution of the correlation coefficient (ρ) is shown in gray, while the expected speed up is shown for 100× (green curve) and 10× (yellow curve) selectivity optimization. The inserted box shows the mean and 95% confidence interval for the correlation coefficient. The marginal distribution of speedup is shown on the right side of the plot for both 100× (green) and 10× (yellow) selectivity optimization speedups. (**B**) As above, but for the more closely related CDK2/CDK9 selectivity dataset.

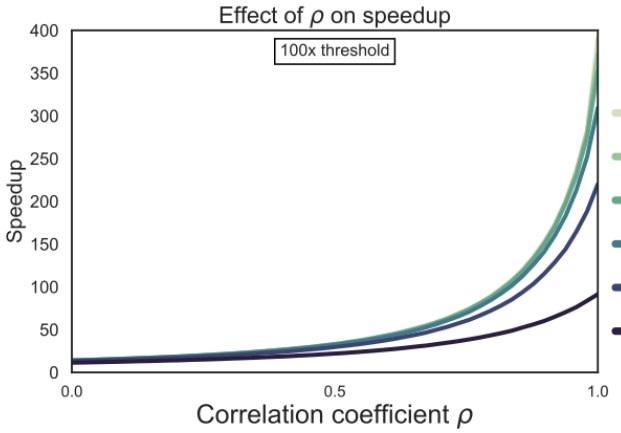

σ_{stat} (kcal/mol)	Effort
0	∞
0.025	48
0.05	16
0.1	4
0.2	1
0.4	1/4

Figure 6. Correlation in selectivity prediction errors can be used to accelerate selectivity optimization
(**A**) (*left*) The joint posterior distribution of the prediction errors for CDK2 (X-axis) and ERK2 (Y-axis) from the Bayesian graphical model. (*right*) Speedup in selectivity optimization (Y-axis) as a function of correlation coefficient (X-axis). The posterior marginal distribution of the correlation coefficient (ρ) is shown in gray, while the expected speed up is shown for 100x (green curve) and 10x (yellow curve) selectivity optimization. The inserted box shows the mean and 95% confidence interval for the correlation coefficient. The marginal distribution of speedup is shown on the right side of the plot for both 100x (green) and 10x (yellow) selectivity optimization speedups. (**B**) (*left*) The same as above, with CDK2 (X-axis) and CDK9 (Y-axis). (*right*) As above, for the CDK2/CDK9 calculations.

Expending more effort to reduce statistical error can improve selectivity optimization speedups

To this point, we have considered only forcefield error in quantifying the speedup free energy calculations can enable for selectivity optimization, by assuming we are in the range of infinite sampling, where the statistical error for each target is reduced to 0 kcal/mol. To begin understanding how statistical error impacts this speedup, we modified the model of speedup by additionally considering the per target statistical error (σ_{stat}), which we define in Equation 4 such that at the baseline effort, N, σ_{stat} is 0.2 kcal/mol. In this definition, it takes 4 times the sampling, or effort, to reduce statistical error by a factor of 2. We assume that statistical error is uncorrelated when propagating to two targets, and that σ_{ff} is 0.9 kcal/mol for both targets [57, 59]. As shown in Figure 5, expending effort to reduce σ_{stat} when ρ is less than 0.5 does not change the expected speedup for the 100x threshold in meaningful way, suggesting that it is not worth running calculations longer than the default protocol in this case. However, when ρ is greeter than 0.5, the curves do start to separate, particularly the 1/4x, 1x and 4x effort curves. This suggests that when the correlation is high, running longer calculations can net improvements in selectivity optimization speed. Interestingly, the 16x, 48x and ∞ effort curves do not differ greatly from the 4x effort curve, indicating that there are diminishing returns to running longer calculations.

In order to understand what the current statistical error is for our calculations, we performed three replicates of our calculations, and calculated the standard deviation of the cycle closure $\Delta\Delta G$ for each edge of the map, and compared that value to the cycle closure errors reported for each edge (Supp. Figure 9). In general, the standard deviation suggests that the statistical error for our calculations is between 0.1 and 0.3 kcal/mol. While this does not agree well with the cycle closure error (Supp. Figure 9), the high variation of the cycle closure errors between replicates of each edge suggest that the standard deviation is a more reliable estimate of what the statistical error for these calculations is.

Discussion and Conclusions

There are a number of different metrics for quantifying the selectivity of a compound [54], which look at selectivity from different views depending on the information trying to be conveyed. One of the earliest metrics was the standard selectivity score, which conveyed the number of inhibited kinase targets in a broad scale assay divided by the total number of kinases in the assay [60]. The gini coefficient is a method that does not rely on any threshold, but is highly sensitive to experimental conditions because it is dependent on

percent inhibition [61]. Other metrics take a thermodynamic approach to kinase selectivity and are suitable for smaller panel screens [62, 63]. Here, we propose a more granular, thermodynamic view of selectivity that is easy to use free energy methods to calculate: the change in free energy of binding for a given ligand between two different targets ($\Delta\Delta G_{selectivity}$). $\Delta\Delta G_{selectivity}$ is a useful metric of selectivity in lead optimization once a single, or small panel, of off-targets have been identified and the goal is to use physical modeling to either improve or maintain selectivity within a lead series.

We have demonstrated, using a simple numerical model, the impact that free energy calculations with even weakly correlated forcefield errors can have on speeding up the optimization of selectivity in small molecule kinase inhibitors. While the expected speed up is dependent on the per target forcefield error of the method (σ_{ff}), the speedup is also highly dependent on the correlation of errors made for both targets. Unsurprisingly, free energy methods have greater impact as the threshold for selectivity optimization goes from 10x to 100x. While 100x selectivity optimization is difficult to achieve, the expected benefit from free energy calculations is also quite high, with 1 and 2 order of magnitude speedups possible.

To quantify the correlation of errors in two example systems, we gathered experimental data for two congeneric ligand series with experimental data for CDK2 and ERK2, as well as CDK2 and CDK9. These datasets, which had crystal structures for both targets with the same ligand co-crystallized, exemplify the difficulty in predicting selectivity. The dynamic range of selectivity for both systems is incredibly narrow, with most of the perturbations not having a major impact on the overall selectivity achieved. Further, the data was reported with unrelaible experimental uncertainties, which makes quantifying the errors made by the free energy calculations difficult. This issue is common when considering selectivity, as many kinase-oriented high throughput screens are carried out at a single concentration and not highly quantitative. Despite CDK2 and ERK2 being more distantly related than CDK2 and CDK9, the calculated correlation in the forcefield error suggests that fortuitous cancellation of errors may be applicable in a wider range of scenarios than closely related kinases within the same family.

We built a numerical model of the impact of statistical error in the context of different levels of forcefield error correlation, in order to better understand if there are situations where it is beneficial to expend more effort running longer calculations to minimize statistical error and get improved speedup in selectivity optimization. Our results suggest that unless the correlation is above 0.5 for the two targets of interest, there is not much benefit in running longer calculations. However, when the forcefield error is reduced by correlation, longer calculations can help realized large increases in speedup. Keeping a running quantification of ρ for free energy calculations as compounds are made and the predictions can be tested will allow for decisions to be made about whether running longer calculations is worthwhile. It will also allow for an estimate of $\sigma_{selectivity}$, which is useful for estimating expected forcefield error for prospective predictions. Importantly, we expect that correlation will be protocol dependent and changes to the way the system is modeled are expected to change the observed correlation in the forcefield error.

This work demonstrates that correlation in the forcefield errors can allow free energy calculations to facilitate significant speedups in selectivity optimization for drug discovery projects. This is particularly important in kinase systems, where considering multiple targets is an important part of the process. The results suggest that free energy calculations can be particularly helpful in the design of kinase polypharmacological agents, especially in cases where there is high correlation in the forcefield errors between multiple targets.

Methods

Numerical model of selectivity optimization speedup

To model the impact correlation of forcefield error would have on the expected uncertainty for selectivity predictions in the regime of infinite sampling and zero statistical error, $\sigma_{\text{selectivity}}$ was calculated using Equation 2 for 1000 evenly spaced values of the correlation coefficient (ρ) from 0 to 1, for a number of combinations of per target forcefield errors ($\sigma_{\text{ff},1}$ and $\sigma_{\text{ff},2}$)

$$\sigma_{\text{selectivity}} = \sqrt{\sigma_{\text{ff},1}^2 + \sigma_{\text{ff},2}^2 - 2\rho\,\sigma_{\text{ff},1}\,\sigma_{\text{ff},2}} \tag{2}$$

The speed up in selectivity optimization that could be expected from using free energy calculations of a particular per target error ($\sigma_{\text{selectivity}}$) was quantified as follows using NumPy (v 1.14.2). An original, true

distribution for the change in selectivity of 200 000 000 new compounds proposed with respect to a reference compound was modeled as a normal distribution centered around 0 with a standard deviation of 1 kcal/mol. This assumption was made on the basis that the majority of selectivity is driven by the scaffold, and R group modifications will do little to drive changes in selectivity. The 1 kcal/mol distribution is supported by the standard deviations of the selectivity in the experimental datasets referenced in this work, which are all less than, but close, to 1 kcal/mol.

Each of these proposed compounds were "screened" by a free energy calculation technique with a per target forcefield error (σ_{ff}) of 1 kcal/mol and a specified correlation coefficient ρ. A $\sigma_{\text{selectivity}}$ was calculated according to Equation 2. The noise of the computational method was modeled as a normal distribution centered around 0 with a standard deviation of $\sigma_{\text{selectivity}}$ and added to the "true" change in selectivity, giving us the predicted change in selectivity ($\Delta S_{\text{compound}}$). This process can be described by Equation 3:

$$\Delta S_{\text{compound}} = \mathcal{N}_{\text{true}}(\mu = 0, \sigma^2 = 1) + \mathcal{N}_{\text{forcefield}}(\mu = 0, \sigma^2_{\text{selectivity}}(\rho)) \tag{3}$$

Any compound predicted to have an improvement in selectivity of 1.4 kcal/mol (1 $\log_{10}$ unit) would then be made and have its selectivity experimental measured, using an experimental method with perfect accuracy. The speedup value for each value of ρ is calculated as the proportion of compounds made with a true selectivity gain of 1.4 kcal/mol divided by the proportion of compounds with a 1.4 kcal/mol improvement in the original distribution, where all of the compounds were made.

This process was repeated for a 100x (2.8 kcal/mol, 2 log unit) selectivity optimization and 50 linearly spaced values of the correlation coefficient (ρ) between 0 and 1, for four values of $\sigma_{\text{selectivity}}$ and 40 000 000 compounds in the original distribution.

Numerical model of impact of statistical error on selectivity optimization

To model the impact of statistical error on selectivity optimization at different levels of correlation in the forcefield error, a similar scheme as above was used. An original, true distribution of 40000000 compounds was proposed with respect to a reference compound, drawing from a normal distribution centered on 0 with a standard deviation of 1 (Numpy v 1.14.2). Each of these proposed compounds were "screened" by a free energy calculation technique with a per target forcefield error (σ_{ff}) of 0.9 kcal/mol [59] and a specified correlation coefficient ρ, which was evenly spaced between 0 and 1 in 50 steps. A $\sigma_{\text{selectivity}}$ was calculated according to Equation 2. Additionally, a per target statistical error (σ_{stat}) was as in Equation 4

$$\sigma_{\text{stat}} = \sqrt{\frac{2\sigma^2}{N}} \tag{4}$$

Where N is the effort put into running sampling the calculation and σ is such that when N is 1, σ_{stat} = 0.2 kcal/mol. The statistical error was propagated assuming it was uncorrelated, such as in Equation 2 where ρ = 0, giving us $\sigma_{\text{statistics}}$ The forcefield and statistical errors where modeled as Gaussian noise added to the true distribution, as in Equation 5.

$$\Delta S_{\text{compound}} = \mathcal{N}_{\text{true}}(\mu = 0, \sigma^2 = 1) + \mathcal{N}_{\text{forcefield}}(\mu = 0, \sigma^2_{\text{selectivity}}(\rho)) + \mathcal{N}_{\text{stat}}(\mu = 0, \sigma^2_{\text{statistics}}(\rho)) \tag{5}$$

Any compound predicted to have an improvement in selectivity of 2.8 kcal/mol (2 log units) would then be made and have its selectivity experimental measured, using an experimental method with perfect accuracy. The speedup value for each value of ρ is calculated as the proportion of compounds made with a true selectivity gain of 2.8 kcal/mol divided by the proportion of compounds with a 2.8 kcal/mol improvement in the original distribution, where all of the compounds were made.

Structure Preparation

Structures from the Shao [52] and Hole [56], and Blake [53] papers were downloaded from the PDB [64],selecting structures with the same co-ligand crystallized. For the Shao dataset, 4BCK (CDK2) and 4BCI (CDK9) were selected, which have ligand 12c cocrystallized. For the Blake dataset, 5K4J (CDK2) and 5K4I (ERK2) were selected, cocrystallized with ligand 21. The structures were prepared using Schrodinger's Protein Preparation Wizard [65] (release 2017-3). This pipeline modeled in internal loops and missing atoms, added hydrogens at

the reported experimental pH (7.0 for the Shao dataset, 7.3 for the Blake dataset) for both the protein and the ligand. All crystal waters were retained. The ligand was assigned protonation and tautomer states using Epik at the experimental pH±2, and hydrogen bonding was optimized using PROPKA at the experimental pH±2. Finally, the entire structure was minimized using OPLS3 with an RMSD cutoff of 0.3Å.

Ligand Pose Generation

Ligands were extracted from the publication entries in the BindingDB as 2D SMILES strings. 3D conformations were generated using LigPrep with OPLS3 [59]. Ionization state was assigned using Epik at experimental pH±2. Stereoisomers were computed by retaining any specified chiralities and varying the rest. The tautomer and ionization state with the lowest epik state penalty was selected for use in the calculation. Any ligands predicted to have a positive or negative charge in its lowest Epik state penalty was excluded, with the exception of Compound 9 from the Blake dataset. This ligand was predicted to have a +1 charge for its lowest state penalty state. The neutral form the ligand was include for the sake of cycle closure in the FEP+ map, but was ignored for the sake any analysis afterwards. Ligand poses were generated by first aligning to the co-crystal ligand using the Largest Common Bemis-Murcko scaffold with fuzzy matching (Schrodinger 2017-4). Ligands that were poorly aligned or failed to align were then aligned using Maximum Common Substructure (MCSS). Finally, large R-groups were allowed to sample different conformations using MM-GBSA with a common core restrained. VSGB solvation model was used with the OPLS3 forcefield. No flexible residues were defined for the ligand.

Free Energy Calculations

The FEP+ panel (Maestro release 2017-4) was used to generate perturbation maps. FEP+ calculations were run using the FEP+ panel from Maestro release 2018-3, using the parameters from the version of OPLS3e that shipped with the 2018-3 release. Any missing ligand torsions were fit using the automated FFbuilder protocol [66]. Custom charges were assigned using the OPLS3e forcefield using input geometries, according to the automated FEP+ workflow released in 2018-3. Neutral perturbations were run for 15ns per replica, using an NPT ensemble and water buffer size of 5Å. The SPC water model was used. A GCMC solvation protocol was used to sample buried water molecules in the binding pocket prior to the calculation, which discards any retained crystal waters.

Statistical Analysis of FEP+ calculations

Each FEP+ calculation has a reported mean unsigned error (MUE) and root mean squared error (RMSE) with a bootstrapped 95% confidence interval. The MUE was calculated according Equation 6, while the RMSE was calculated according to Equation 7.

$$MUE = \frac{\sum_0^n \mid \Delta G_{\text{calc}} - \Delta G_{\text{exp}} \mid}{n} \tag{6}$$

$$RMSE = \frac{\sum_0^n \sqrt{\Delta\, G_{\text{calc}}^2 - \Delta\, G_{\text{exp}}^2}}{n} \tag{7}$$

Each RMSE and MUE is reported with a 95% confidence interval calculated from 10000 replicates of a choose-one-replace bootstrap protocol on the ΔG values reported to account for the finite sample size of the ligands. The code used to bootstrap these values is available on github: https://github.com/choderalab/selectivity

Quantification of the correlation coefficient ρ

To quantify ρ, we built a Bayesian graphical model using pymc3 (v. 3.5) [67] and theano (v 1.0.3) [68], which has been made available on Github. For each phase (complex and solvent), the absolute free energy (G) of ligand i was treated as a normal distribution (Equation 8). For each set of calculations, one ligand was chosen as the reference, and pinned to 0, with a standard deviation of 1 kcal/mol in order to improve the efficiency of sampling from the model.

$$G_{i,\text{target}}^{phase} = \mathcal{N}(\text{mean} = 0,\ \text{sd} = 25.0\ \text{kcal/mol}) \tag{8}$$

For each edge of the FEP map (ligand i –> ligand j), there is a contribution from dummy atoms, that was modeled as in Equation 9.

$$c_{i,j} = \mathcal{N}(\text{mean} = 0,\ \text{sd} = 25.0\ \text{kcal/mol}) \tag{9}$$

The model was conditioned by including data from the FEP+ calculation.

$$\Delta G^{\text{BAR}}_{\text{phase},\ ij,\ \text{target}} = \mathcal{N}(G^{\text{phase}}_{j,\text{target}} - G^{\text{phase}}_{i,\text{target}},\ \delta^2 \Delta G^{\text{BAR}}_{\text{phase},\ ij,\ \text{target}},\ \text{observed} = \Delta G^{\text{calc}}_{\text{phase},\ ij,\ \text{target}}) \tag{10}$$

where $\delta^2 \Delta G^{\text{BAR}}_{\text{phase},\ ij,\ \text{target}}$ is the reported BAR uncertainty from the calculation, and $\Delta G^{\text{calc}}_{\text{phase},\ ij,\ \text{target}}$ is the BAR estimate of the free energy for the perturbation between ligands i and j in a given phase.

From this, we can calculate the $\Delta\Delta G^{\text{FEP}}$ for each edge as in Equation 11:

$$\Delta\Delta G^{\text{FEP}}_{\text{target},\ ij} = \Delta G^{\text{BAR}}_{\text{complex},\ ij,\ target} - \Delta G^{\text{BAR}}_{\text{solvent},\ ij,\ target} \tag{11}$$

To model the way an offset is calculated for the $\Delta\ G$ reported by the FEP+ panel in Maestro, we include:

$$\text{offset} = \frac{\sum^n G^{\text{complex}}_{i,\text{target}} - G^{\text{solvent}}_{i,\text{target}}}{n} - \frac{\sum^n \Delta G^{\text{exp}}_i}{n} \tag{12}$$

The offset was added to each ΔG^{BAR}_i to calculate ΔG^{sch}_i.

The experimental binding affinity was treated as a true value ($\Delta G^{\text{true}}_{i,\text{target}}$) corrupted by experimental uncertainty, which is assumed to be 0.3 kcal/mol [6]. There are a number of studies that report on the reproducibility and uncertainty of intralab IC50 measurements, ranging from as small as 0.22 kcal/mol [57] to as high as 0.4 kcal/mol [6]. The assumed value falls within this range and is in good agreement with the uncertainty reported from multiple replicate measurements in internal datasets at Novartis [69].

The values reported in the papers ($\Delta G^{\text{obs}}_{i,\text{target}}$) were treated as observations from this distribution (Equation 13),

$$\Delta G^{\text{exp}}_{i,\text{target}} = \mathcal{N}(\text{mean} = \Delta G^{true}_{i,\text{target}},\ \text{sd} = 0.3\ \text{kcal/mol},\ \text{observed} = \Delta G^{\text{obs}}_{i,\text{target}}) \tag{13}$$

$\Delta G^{\text{true}}_{i,\text{target}}$ was assigned a weak normal prior, as in Equation 14,

$$\Delta G^{\text{true}}_{i,\text{target}} = \mathcal{N}(\text{mean} = 0,\ \text{sd} = 50\ \text{kcal/mol}). \tag{14}$$

The error for a given ligand was calculated as in Equation 15.

$$\epsilon_i = \Delta G^{\text{sch}}_i - \Delta G^{\text{true}}_i \tag{15}$$

From these ϵ values, we calculated the correlation coefficient, ρ as in Equation 16.

$$\rho = \frac{cov(\epsilon_{\text{target1}}, \epsilon_{\text{target2}})}{\sigma_{\text{target 1}} \sigma_{\text{target 2}}} \tag{16}$$

where σ is the standard deviation of ϵ.

To quantify ρ from these calculations, the default NUTS sampler with `jitter+adapt_diag` initialization, 3 000 tuning steps, and the default target accept probability was used to draw 20 000 samples from the model.

Calculating the marginal distribution of speedup

To quantify the expected speedup from the calculations we ran, we utilized 10000 replicates of the scheme detailed above to calculate speedup given parameters ρ, $\sigma_{ff,1}$ and $\sigma_{ff,2}$, in the regime of infinite effort and zero statistical error. Using Numpy (v 1.14.2), ρ was drawn from a normal distribution with the mean and standard deviation from the posterior distribution of ρ from the Bayesian Graphical model. The per target forcefield errors, $\sigma_{ff,1}$ and $\sigma_{ff,2}$, were estimated from the mean of the absolute value of $\epsilon_{target1}$ and $\epsilon_{target2}$, which are the magnitude of errors from the Bayesian graphical model. $\sigma_{selectivity}$ was calculated using Equation 2. 100000 molecules were proposed from true normal distribution, as above. The error of the computational method was modeled as in Equation 3.

Acknowledgments

The authors are grateful to Patrick Grinaway (ORCID: 0000-0002-9762-4201) for useful discussions about Bayesian statistics and Mehtap Işık (ORCID: 0000-0002-6789-952X) for useful discussion about kinase inhibitor protonation states. SKA is grateful to Haoyu S. Yu, Wei Chen, and Dmitry Lupyan for advice on running FEP+ calculations.

JDC: Add more acknowledgments here.

Funding

Research reported in this publication was supported by the National Institute for General Medical Sciences of the National Institutes of Health under award numbers R01GM121505 and P30CA008748. SKA acknowledges financial support from Schrödinger and the Sloan Kettering Institute. JDC acknowledges financial support from Cycle for Survival and the Sloan Kettering Institute.

Disclosures

JDC was a member of the Scientific Advisory Board for Schrödinger, LLC during part of this study. JDC is a current member of the Scientific Advisory Board of OpenEye Scientific Software. The Chodera laboratory receives or has received funding from multiple sources, including the National Institutes of Health, the National Science Foundation, the Parker Institute for Cancer Immunotherapy, Relay Therapeutics, Entasis Therapeutics, Silicon Therapeutics, EMD Serono (Merck KGaA), AstraZeneca, XtalPi, the Molecular Sciences Software Institute, the Starr Cancer Consortium, the Open Force Field Consortium, Cycle for Survival, a Louis V. Gerstner Young Investigator Award, and the Sloan Kettering Institute. A complete funding history for the Chodera lab can be found at http://choderalab.org/funding

Author Contributions

Conceptualization: SKA, LW, RA, JDC
Methodology: SKA, LW, JDC
Investigation: SKA, SP
Writing – Original Draft: SKA
Writing – Review & Editing: SKA, JDC
Funding Acquisition: RA, JDC
Resources: LW, JDC
Supervision: LW, JDC

References

[1] **Chodera JD**, Mobley DL, Shirts MR, Dixon RW, Branson K, Pande VS. Alchemical free energy methods for drug discovery: progress and challenges. Curr Opin Struct Biol. 2011 Apr; 21(2):150–160.

[2] **Huang J**, MacKerell AD. CHARMM36 All-Atom Additive Protein Force Field: Validation Based on Comparison to NMR Data. J Comput Chem. 2013 Sep; 34(25):2135–2145. doi: 10.1002/jcc.23354.

[3] **Maier JA**, Martinez C, Kasavajhala K, Wickstrom L, Hauser KE, Simmerling C. ff14SB: Improving the Accuracy of Protein Side Chain and Backbone Parameters from ff99SB. J Chem Theory Comput. 2015 Aug; 11(8):3696–3713. doi: 10.1021/acs.jctc.5b00255.

[4] **Harder E**, Damm W, Maple J, Wu C, Reboul M, Xiang JY, Wang L, Lupyan D, Dahlgren MK, Knight JL, Kaus JW, Cerutti DS, Krilov G, Jorgensen WL, Abel R, Friesner RA. OPLS3: A Force Field Providing Broad Coverage of Drug-like Small Molecules and Proteins. J Chem Theory Comput. 2016 Jan; 12(1):281–296. doi: 10.1021/acs.jctc.5b00864.

[5] **Cournia Z**, Allen B, Sherman W. Relative Binding Free Energy Calculations in Drug Discovery: Recent Advances and Practical Considerations. Journal of chemical information and modeling. 2017 Dec; 57(12):2911–2937.

[6] **Brown SP**, Muchmore SW, Hajduk PJ. Healthy Skepticism: Assessing Realistic Model Performance. Drug Discov Today. 2009; 14(7):420 – 427. doi: http://dx.doi.org/10.1016/j.drudis.2009.01.012.

[7] **Abel R**, Mondal S, Masse C, Greenwood J, Harriman G, Ashwell MA, Bhat S, Wester R, Frye L, Kapeller R, Friesner RA. Accelerating drug discovery through tight integration of expert molecular design and predictive scoring. Curr Opin Struct Biol. 2017 Apr; 43(Supplement C):38–44.

[8] **Lovering F**, Aevazelis C, Chang J, Dehnhardt C, Fitz L, Han S, Janz K, Lee J, Kaila N, McDonald J, Moore W, Moretto A, Papaioannou N, Richard D, Ryan MS, Wan ZK, Thorarensen A. Imidazotriazines: Spleen Tyrosine Kinase (Syk) Inhibitors Identified by Free-Energy Perturbation (FEP). ChemMedChem. 2016 Jan; 11(2):217–233.

[9] **Ciordia M**, Pérez-Benito L, Delgado F, Trabanco AA, Tresadern G. Application of Free Energy Perturbation for the Design of BACE1 Inhibitors. Journal of chemical information and modeling. 2016 Sep; 56(9):1856–1871.

[10] **Lenselink EB**, Louvel J, Forti AF, van Veldhoven JPD, de Vries H, Mulder-Krieger T, McRobb FM, Negri A, Goose J, Abel R, van Vlijmen HWT, Wang L, Harder E, Sherman W, IJzerman AP, Beuming T. Predicting Binding Affinities for GPCR Ligands Using Free-Energy Perturbation. ACS omega. 2016 Aug; 1(2):293–304.

[11] **Jorgensen WL**. Computer-aided discovery of anti-HIV agents. Bioorganic & medicinal chemistry. 2016 Oct; 24(20):4768–4778.

[12] **Wang L**, Wu Y, Deng Y, Kim B, Pierce L, Krilov G, Lupyan D, Robinson S, Dahlgren MK, Greenwood J, Romero DL, Masse C, Knight JL, Steinbrecher T, Beuming T, Damm W, Harder E, Sherman W, Brewer M, Wester R, et al. Accurate and Reliable Prediction of Relative Ligand Binding Potency in Prospective Drug Discovery by Way of a Modern Free-Energy Calculation Protocol and Force Field. J Am Chem Soc. 2015 Feb; 137(7):2695–2703. doi: 10.1021/ja512751q.

[13] **Abel R**, Wang L, Harder ED, Berne BJ, Friesner RA. Advancing Drug Discovery through Enhanced Free Energy Calculations. Accounts of chemical research. 2017 Jul; 50(7):1625–1632.

[14] **Zhang J**, Yang PL, Gray NS. Targeting cancer with small molecule kinase inhibitors. Nat Rev Cancer. 2009 Jan; 9(1):28–39.

[15] **Huggins DJ**, Sherman W, Tidor B. Rational approaches to improving selectivity in drug design. J Med Chem. 2012 Feb; 55(4):1424–1444.

[16] **Fan QW**, Cheng CK, Nicolaides TP, Hackett CS, Knight ZA, Shokat KM, Weiss WA. A dual phosphoinositide-3-kinase alpha/mTOR inhibitor cooperates with blockade of epidermal growth factor receptor in PTEN-mutant glioma. Cancer Res. 2007 Sep; 67(17):7960–7965.

[17] **Apsel B**, Blair JA, Gonzalez B, Nazif TM, Feldman ME, Aizenstein B, Hoffman R, Williams RL, Shokat KM, Knight ZA. Targeted polypharmacology: discovery of dual inhibitors of tyrosine and phosphoinositide kinases. Nat Chem Biol. 2008 Nov; 4(11):691–699.

[18] **Knight ZA**, Lin H, Shokat KM. Targeting the Cancer Kinome through Polypharmacology. Nat Rev Cancer. 2010; 10(2):130.

[19] **Hopkins AL**, Mason JS, Overington JP. Can we rationally design promiscuous drugs? Curr Opin Struct Biol. 2006 Feb; 16(1):127–136.

[20] **Hopkins AL**. Network pharmacology: the next paradigm in drug discovery. Nat Chem Biol. 2008 Nov; 4(11):682–690.

[21] **Kijima T**, Shimizu T, Nonen S, Furukawa M, Otani Y, Minami T, Takahashi R, Hirata H, Nagatomo I, Takeda Y, Kida H, Goya S, Fujio Y, Azuma J, Tachibana I, Kawase I. Safe and successful treatment with erlotinib after gefitinib-induced hepatotoxicity: difference in metabolism as a possible mechanism. J Clin Oncol. 2011 Jul; 29(19):e588–90.

[22] **Liu S**, Kurzrock R. Toxicity of targeted therapy: Implications for response and impact of genetic polymorphisms. Cancer Treat Rev. 2014 Aug; 40(7):883–891.

[23] **Rudmann DG**. On-target and off-target-based toxicologic effects. Toxicol Pathol. 2013 Feb; 41(2):310–314.

[24] **Mendoza MC**, Er EE, Blenis J. The Ras-ERK and PI3K-mTOR pathways: cross-talk and compensation. Trends Biochem Sci. 2011 Jun; 36(6):320–328.

[25] **Tricker EM**, Xu C, Uddin S, Capelletti M, Ercan D, Ogino A, Pratilas CA, Rosen N, Gray NS, Wong KK, Jänne PA. Combined EGFR/MEK Inhibition Prevents the Emergence of Resistance in EGFR-Mutant Lung Cancer. Cancer Discov. 2015 Sep; 5(9):960–971.

[26] **Bailey ST**, Zhou B, Damrauer JS, Krishnan B, Wilson HL, Smith AM, Li M, Yeh JJ, Kim WY. mTOR Inhibition Induces Compensatory, Therapeutically Targetable MEK Activation in Renal Cell Carcinoma. PLoS One. 2014 Sep; 9(9):e104413.

[27] **Chandarlapaty S**, Sawai A, Scaltriti M, Rodrik-Outmezguine V, Grbovic-Huezo O, Serra V, Majumder PK, Baselga J, Rosen N. AKT Inhibition Relieves Feedback Suppression of Receptor Tyrosine Kinase Expression and Activity. Cancer Cell. 2011 Jan; 19(1):58–71. doi: 10.1016/j.ccr.2010.10.031.

[28] **Pao W**, Miller V, Zakowski M, Doherty J, Politi K, Sarkaria I, Singh B, Heelan R, Rusch V, Fulton L, Mardis E, Kupfer D, Wilson R, Kris M, Varmus H. EGF receptor gene mutations are common in lung cancers from "never smokers" and are associated with sensitivity of tumors to gefitinib and erlotinib. Proceedings of the National Academy of Sciences. 2004 Sep; 101(36):13306–13311.

[29] **Kim Y**, Li Z, Apetri M, Luo B, Settleman JE, Anderson KS. Temporal resolution of autophosphorylation for normal and oncogenic forms of EGFR and differential effects of gefitinib. Biochemistry. 2012 Jun; 51(25):5212–5222.

[30] **Juchum M**, Günther M, Laufer SA. Fighting Cancer Drug Resistance: Opportunities and Challenges for Mutation-Specific EGFR Inhibitors. Drug Resist Updat. 2015 May; 20:12–28. doi: 10.1016/j.drup.2015.05.002.

[31] **Din OS**, Woll PJ. Treatment of gastrointestinal stromal tumor: focus on imatinib mesylate. Ther Clin Risk Manag. 2008 Feb; 4(1):149–162.

[32] **Lin YL**, Meng Y, Jiang W, Roux B. Explaining why Gleevec is a specific and potent inhibitor of Abl kinase. Proc Natl Acad Sci U S A. 2013 Jan; 110(5):1664–1669.

[33] **Lin YL**, Meng Y, Huang L, Roux B. Computational Study of Gleevec and G6G Reveals Molecular Determinants of Kinase Inhibitor Selectivity. J Am Chem Soc. 2014 Oct; 136(42):14753–14762.

[34] **Lin YL**, Roux B. Computational Analysis of the Binding Specificity of Gleevec to Abl, c-Kit, Lck, and c-Src Tyrosine Kinases. J Am Chem Soc. 2013 Oct; 135(39):14741–14753.

[35] **Aldeghi M**, Heifetz A, Bodkin MJ, Knapp S, Biggin PC. Predictions of Ligand Selectivity from Absolute Binding Free Energy Calculations. J Am Chem Soc. 2017 Jan; 139(2):946–957.

[36] **Robert Roskoski Jr**. USFDA Approved Protein Kinase Inhibitors. . 2017; http://www.brimr.org/PKI/PKIs.htm, updated 3 May 2017.

[37] **Santos R**, Ursu O, Gaulton A, Bento AP, Donadi RS, Bologa CG, Karlsson A, Al-Lazikani B, Hersey A, Oprea TI, Overington JP. A Comprehensive Map of Molecular Drug Targets. Nat Rev Drug Discov. 2016 Dec; 16(1):19–34. doi: 10.1038/nrd.2016.230.

[38] **Volkamer A**, Eid S, Turk S, Jaeger S, Rippmann F, Fulle S. Pocketome of human kinases: prioritizing the ATP binding sites of (yet) untapped protein kinases for drug discovery. J Chem Inf Model. 2015 Mar; 55(3):538–549.

[39] **Manning G**, Whyte DB, Martinez R, Hunter T, Sudarsanam S. The Protein Kinase Complement of the Human Genome. Science. 2002 Dec; 298(5600):1912–1934.

[40] **Wu P**, Nielsen TE, Clausen MH. FDA-approved small-molecule kinase inhibitors. Trends Pharmacol Sci. 2015 Jul; 36(7):422–439.

[41] **Cowan-Jacob SW**, Fendrich G, Floersheimer A, Furet P, Liebetanz J, Rummel G, Rheinberger P, Centeleghe M, Fabbro D, Manley PW, IUCr. Structural biology contributions to the discovery of drugs to treat chronic myelogenous leukaemia. Acta Crystallogr D Biol Crystallogr. 2007 Jan; 63(1):80–93.

[42] **Seeliger MA**, Nagar B, Frank F, Cao X, Henderson MN, Kuriyan J. c-Src Binds to the Cancer Drug Imatinib with an Inactive Abl/c-Kit Conformation and a Distributed Thermodynamic Penalty. Structure. 2007 Mar; 15(3):299–311.

[43] **Huse M**, Kuriyan J. The conformational plasticity of protein kinases. Cell. 2002 Jan; 109(3):275–282.

[44] **Harrison SC**. Variation on an Src-like theme. Cell. 2003 Mar; 112(6):737–740.

[45] **Volkamer A**, Eid S, Turk S, Rippmann F, Fulle S. Identification and Visualization of Kinase-Specific Subpockets. J Chem Inf Model. 2016 Feb; 56(2):335–346.

[46] **Christmann-Franck S**, van Westen GJP, Papadatos G, Beltran Escudie F, Roberts A, Overington JP, Domine D. Unprecedently Large-Scale Kinase Inhibitor Set Enabling the Accurate Prediction of Compound–Kinase Activities: A Way toward Selective Promiscuity by Design? Journal of chemical information and modeling. 2016 Sep; 56(9):1654–1675.

[47] **Anastassiadis T**, Deacon SW, Devarajan K, Ma H, Peterson JR. Comprehensive assay of kinase catalytic activity reveals features of kinase inhibitor selectivity. Nat Biotechnol. 2011 Nov; 29(11):1039–1045.

[48] **Davis MI**, Hunt JP, Herrgard S, Ciceri P, Wodicka LM, Pallares G, Hocker M, Treiber DK, Zarrinkar PP. Comprehensive Analysis of Kinase Inhibitor Selectivity. Nat Biotechnol. 2011 Oct; 29(11):1046–1051. doi: 10.1038/nbt.1990.

[49] **Klaeger S**, Heinzlmeir S, Wilhelm M, Polzer H, Vick B, Koenig PA, Reinecke M, Ruprecht B, Petzoldt S, Meng C, Zecha J, Reiter K, Qiao H, Helm D, Koch H, Schoof M, Canevari G, Casale E, Depaolini SR, Feuchtinger A, et al. The target landscape of clinical kinase drugs. Science. 2017 Dec; 358(6367).

[50] **Sun C**, Hobor S, Bertotti A, Zecchin D, Huang S, Galimi F, Cottino F, Prahallad A, Grernrum W, Tzani A, Schlicker A, Wessels LFA, Smit EF, Thunnissen E, Halonen P, Lieftink C, Beijersbergen RL, Di Nicolantonio F, Bardelli A, Trusolino L, et al. Intrinsic resistance to MEK inhibition in KRAS mutant lung and colon cancer through transcriptional induction of ERBB3. CellReports. 2014 Apr; 7(1):86–93.

[51] **Manchado E**, Weissmueller S, Morris JP, Chen CC, Wullenkord R, Lujambio A, de Stanchina E, Poirier JT, Gainor JF, Corcoran RB, Engelman JA, Rudin CM, Rosen N, Lowe SW. A combinatorial strategy for treating KRAS-mutant lung cancer. Nature. 2016 Jun; 534(7609):647–651.

[52] **Shao H**, Shi S, Huang S, Hole AJ, Abbas AY, Baumli S, Liu X, Lam F, Foley DW, Fischer PM, Noble M, Endicott JA, Pepper C, Wang S. Substituted 4-(Thiazol-5-yl)-2-(phenylamino)pyrimidines Are Highly Active CDK9 Inhibitors: Synthesis, X-ray Crystal Structures, Structure–Activity Relationship, and Anticancer Activities. J Med Chem. 2013 Feb; 56(3):640–659.

[53] **Blake JF**, Burkard M, Chan J, Chen H, Chou KJ, Diaz D, Dudley DA, Gaudino JJ, Gould SE, Grina J, Hunsaker T, Liu L, Martinson M, Moreno D, Mueller L, Orr C, Pacheco P, Qin A, Rasor K, Ren L, et al. Discovery of (S)-1-(1-(4-Chloro-3-fluorophenyl)-2-hydroxyethyl)-4-(2-((1-methyl-1H-pyrazol-5-yl)amino)pyrimidin-4-yl)pyridin-2(1H)-one (GDC-0994), an Extracellular Signal-Regulated Kinase 1/2 (ERK1/2) Inhibitor in Early Clinical Development. J Med Chem. 2016 Jun; 59(12):5650–5660.

[54] **Bosc N**, Meyer C, Bonnet P. The use of novel selectivity metrics in kinase research. BMC bioinformatics. 2017 Jan; 18(1):17.

[55] **Cheng AC**, Eksterowicz J, Geuns-Meyer S, Sun Y. Analysis of kinase inhibitor selectivity using a thermodynamics-based partition index. J Med Chem. 2010 Jun; 53(11):4502–4510.

[56] **Hole AJ**, Baumli S, Shao H, Shi S, Huang S, Pepper C, Fischer PM, Wang S, Endicott JA, Noble ME. Comparative Structural and Functional Studies of 4-(Thiazol-5-yl)-2-(phenylamino)pyrimidine-5-carbonitrile CDK9 Inhibitors Suggest the Basis for Isotype Selectivity. J Med Chem. 2013 Feb; 56(3):660–670.

[57] **Hauser K**, Negron C, Albanese SK, Ray S, Steinbrecher T, Abel R, Chodera JD, Wang L. Predicting resistance of clinical Abl mutations to targeted kinase inhibitors using alchemical free-energy calculations. Communications Biology. 2018 Jun; 1(1):70.

[58] **Hari SB**, Merritt EA, Maly DJ. Sequence determinants of a specific inactive protein kinase conformation. Chemistry & biology. 2013 Jun; 20(6):806–815.

[59] **Harder E**, Damm W, Maple J, Wu C, Reboul M, Xiang JY, Wang L, Lupyan D, Dahlgren MK, Knight JL, Kaus JW, Cerutti DS, Krilov G, Jorgensen WL, Abel R, Friesner RA. OPLS3: A Force Field Providing Broad Coverage of Drug-like Small Molecules and Proteins. J Chem Theory Comput. 2016 Jan; 12(1):281–296.

[60] **Davis MI**, Hunt JP, Herrgard S, Ciceri P, Wodicka LM, Pallares G, Hocker M, Treiber DK, Zarrinkar PP. Comprehensive analysis of kinase inhibitor selectivity. Nat Biotechnol. 2011 Oct; 29(11):1046–1051.

[61] **Graczyk PP**. Gini coefficient: a new way to express selectivity of kinase inhibitors against a family of kinases. Journal of medicinal chemistry. 2007 Nov; 50(23):5773–5779.

[62] **Duong-Ly KC**, Devarajan K, Liang S, Horiuchi KY, Wang Y, Ma H, Peterson JR. Kinase Inhibitor Profiling Reveals Unexpected Opportunities to Inhibit Disease-Associated Mutant Kinases. CellReports. 2016 Feb; 14(4):772–781.

[63] **Uitdehaag JCM**, Zaman GJR. A theoretical entropy score as a single value to express inhibitor selectivity. BMC bioinformatics. 2011 Apr; 12:94.

[64] **Berman HM**, Battistuz T, Bhat TN, Bluhm WF, Bourne PE, Burkhardt K, Feng Z, Gilliland GL, Iype L, Jain S, Fagan P, Marvin J, Padilla D, Ravichandran V, Schneider B, Thanki N, Weissig H, Westbrook JD, Zardecki C. The Protein Data Bank. Acta Crystallogr D Biol Crystallogr. 2002 Jun; 58(Pt 61):899–907.

[65] **Sastry GM**, Adzhigirey M, Day T, Annabhimoju R, Sherman W. Protein and ligand preparation: parameters, protocols, and influence on virtual screening enrichments. J Comput Aided Mol Des. 2013 Mar; 27(3):221–234.

[66] **Abel R**, Wang L, Harder ED, Berne BJ, Friesner RA. Advancing Drug Discovery through Enhanced Free Energy Calculations. Acc Chem Res. 2017 Jul; 50(7):1625–1632. doi: 10.1021/acs.accounts.7b00083.

[67] **Salvatier J**, Wiecki TV, Fonnesbeck C. Probabilistic programming in Python using PyMC3. PeerJ Computer Science. 2016; 2:e55.

[68] **Al-Rfou R**, Alain G, Almahairi A, Angermueller C, Bahdanau D, Ballas N, Bastien F, Bayer J, Belikov A, Belopolsky A, Bengio Y, Bergeron A, Bergstra J, Bisson V, Bleecher Snyder J, Bouchard N, Boulanger-Lewandowski N, Bouthillier X, de Brébisson A, Breuleux O, et al. Theano: A Python framework for fast computation of mathematical expressions. arXiv e-prints. 2016 May; abs/1605.02688. http://arxiv.org/abs/1605.02688.

[69] **Kalliokoski T**, Kramer C, Vulpetti A, Gedeck P. Comparability of Mixed IC50 Data–a Statistical Analysis. PloS One. 2013; 8(4):e61007.

[70] **Hu J**, Ahuja LG, Meharena HS, Kannan N, Kornev AP, Taylor SS, Shaw AS. Kinase regulation by hydrophobic spine assembly in cancer. Molecular and cellular biology. 2015 Jan; 35(1):264–276.

Supplemental Information

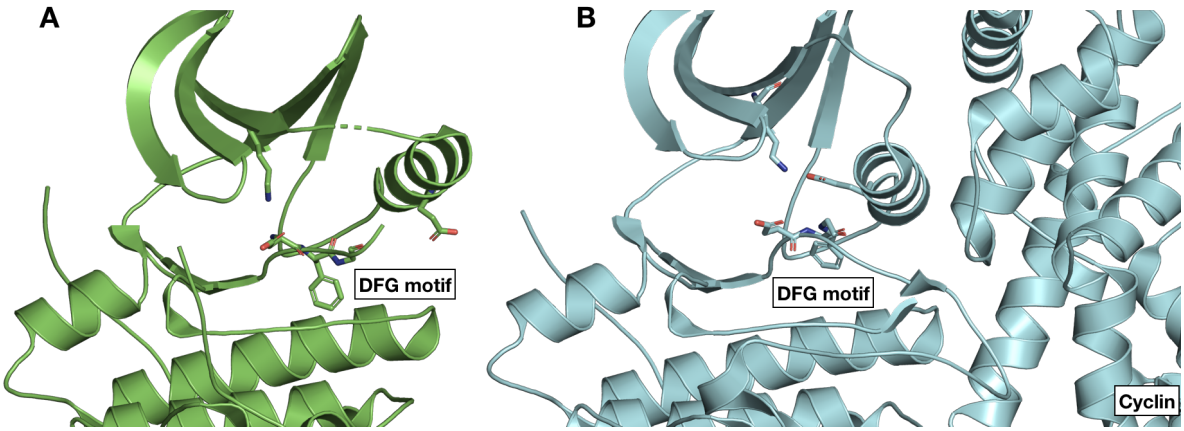

Supplemental Figure. 1. CDK2 adopts an inactive conformation in the crystal structure used for the CDK2/ERK2 calculations
(**A**) CDK2 (5K4J) adopts an inactive conformation in the absence of its cyclin. The DFG motif is in a DFG-in conformation, with the αC helix rotated outwards, breaking the salt bridge between K33 and E51 (Uniprot numbering) that is typically a marker of an active conformation. Notably, the Phe in the DFG motif does not completely form the hydrophobic spine due to the rotation of the αC helix [70] (**B**) The CDK2 structure used for the CDK2/CDK9 calculations (4BCK) contains cyclin A and adopts a DFG-in/αC helix-in conformation that forms the salt bridge between K33 and E51. This is typically indicative of a fully active kinase [43, 58].

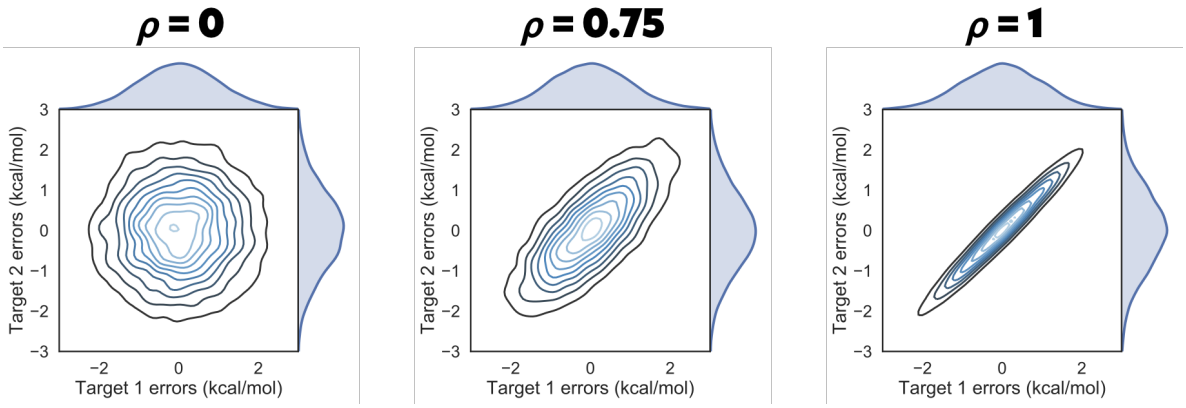

Supplemental Figure. 2. Correlation coefficient ρ controls the shape of the joint marginal distribution of errors
As ρ increases, the joint marginal distribution of errors become more diagonal. Each panel shows 10000 samples drawn from a multivariate normal distribution centered around 0 kcal/mol, where the per target error was set to 1 kcal/mol and ρ to the value indicated in bold over the plot.

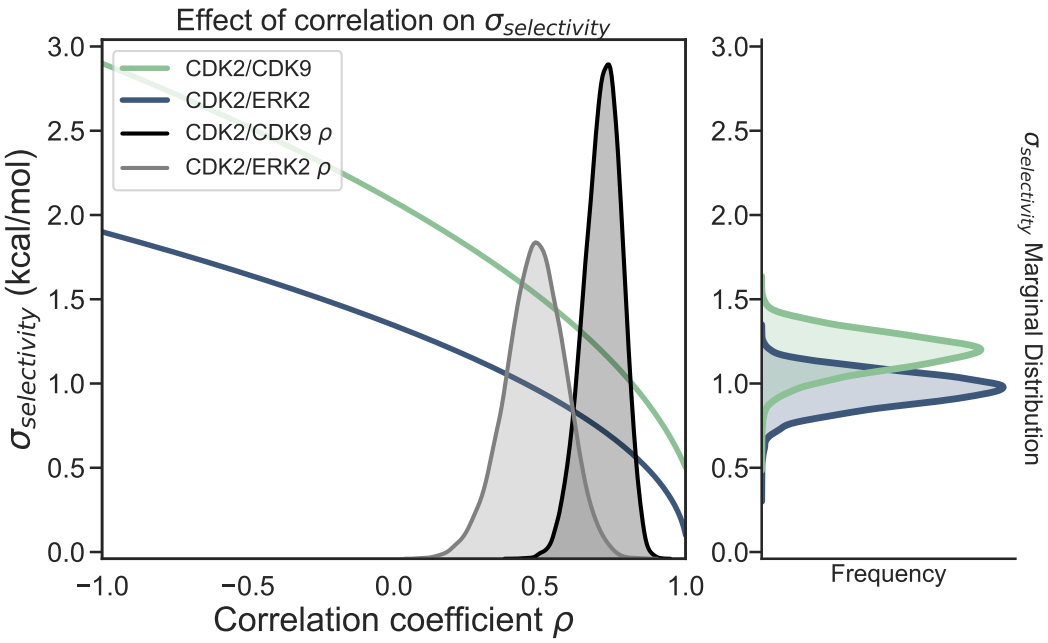

Supplemental Figure. 3. Correlation reduces the expected error for selectivity predictions
As corelation coefficient ρ increases, $\sigma_{selectivity}$ decreases. The intersection between CDK2/CDK9 $\sigma_{selectivity}$ (green curve) and ρ (black distribution) indicates the range of expected $\sigma_{selectivity}$ values. The intersection for CDK2/ERK $\sigma_{selectivity}$ (blue curve) and ρ (gray distribution) suggests the expected $\sigma_{selectivity}$ range for that set of calculations. The right side of the plot shows the marginal distribution for CDK2/CDK9 $\sigma_{selectivity}$ (green curve) and CDK2/ERK $\sigma_{selectivity}$ (blue curve).

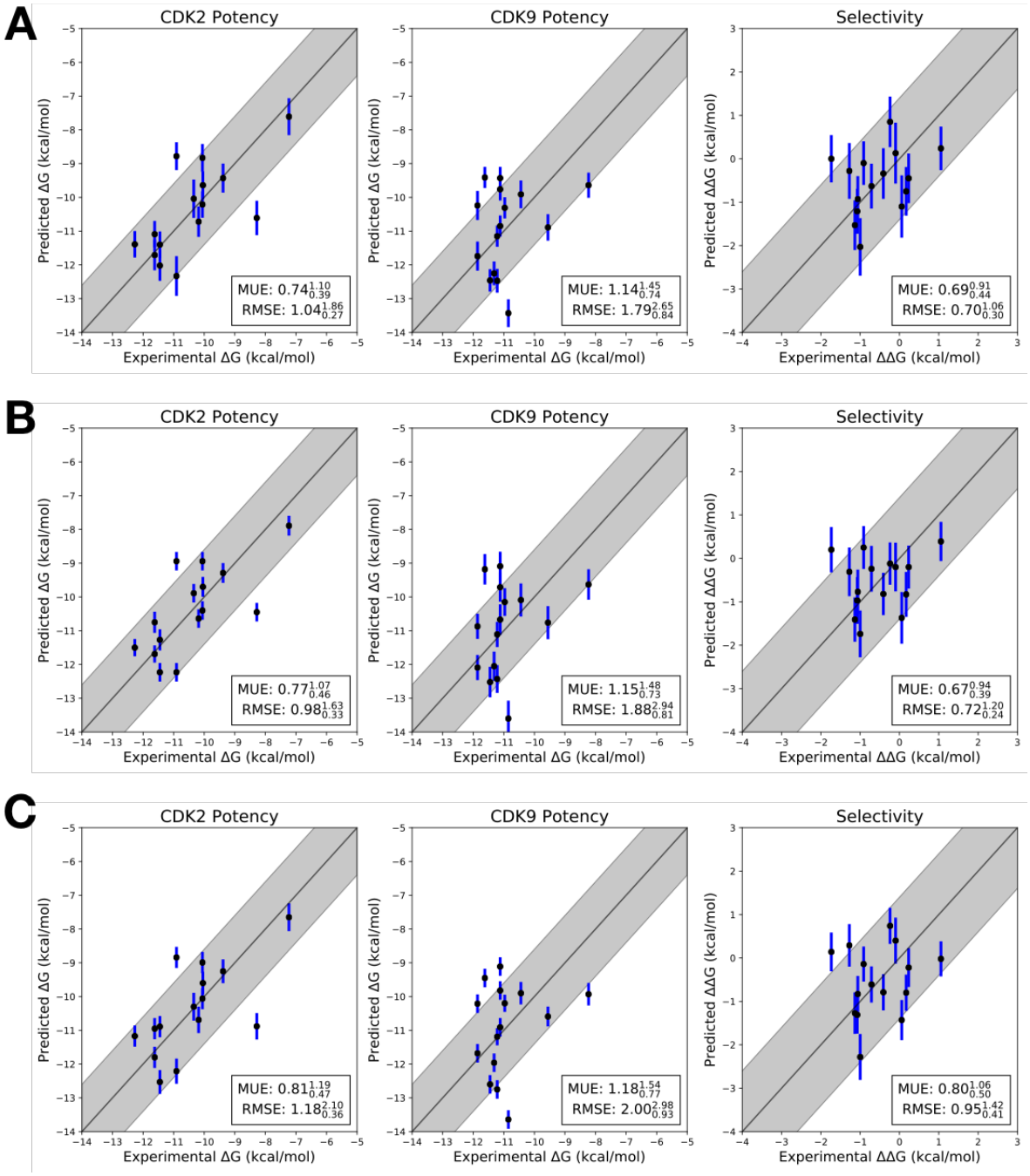

Supplemental Figure. 4. Each replicate of the CDK2/CDK9 calculations yields a consistent RMSE and MUE
Three replicates of the CDK2/CDK9 calculations with different random seeds, but otherwise the same input structures, files, and parameters. The experimental values are shown on the X-axis and calculated values on the Y-axis. Each data point corresponds to a ligand for a given target. All values are shown in units of kcal/mol. The horizontal error bars show the assumed experimental uncertainty of 0.3 kcal/mol[6].We show the 95% CI based on the estimated statistical as vertical blue error bars. For selectivity, the errors were propagated under the assumption that they were completely uncorrelated. The black line indicates agreement between calculation and experiment, while the gray shaded region represent 1.36 kcal/mol (or 1 log unit) error. The MUE and RMSE are shown on each plot with bootstrapped 95% confidence intervals. (**A**) Replicate 1 (**B**) Replicate 2 (**C**) Replicate 3

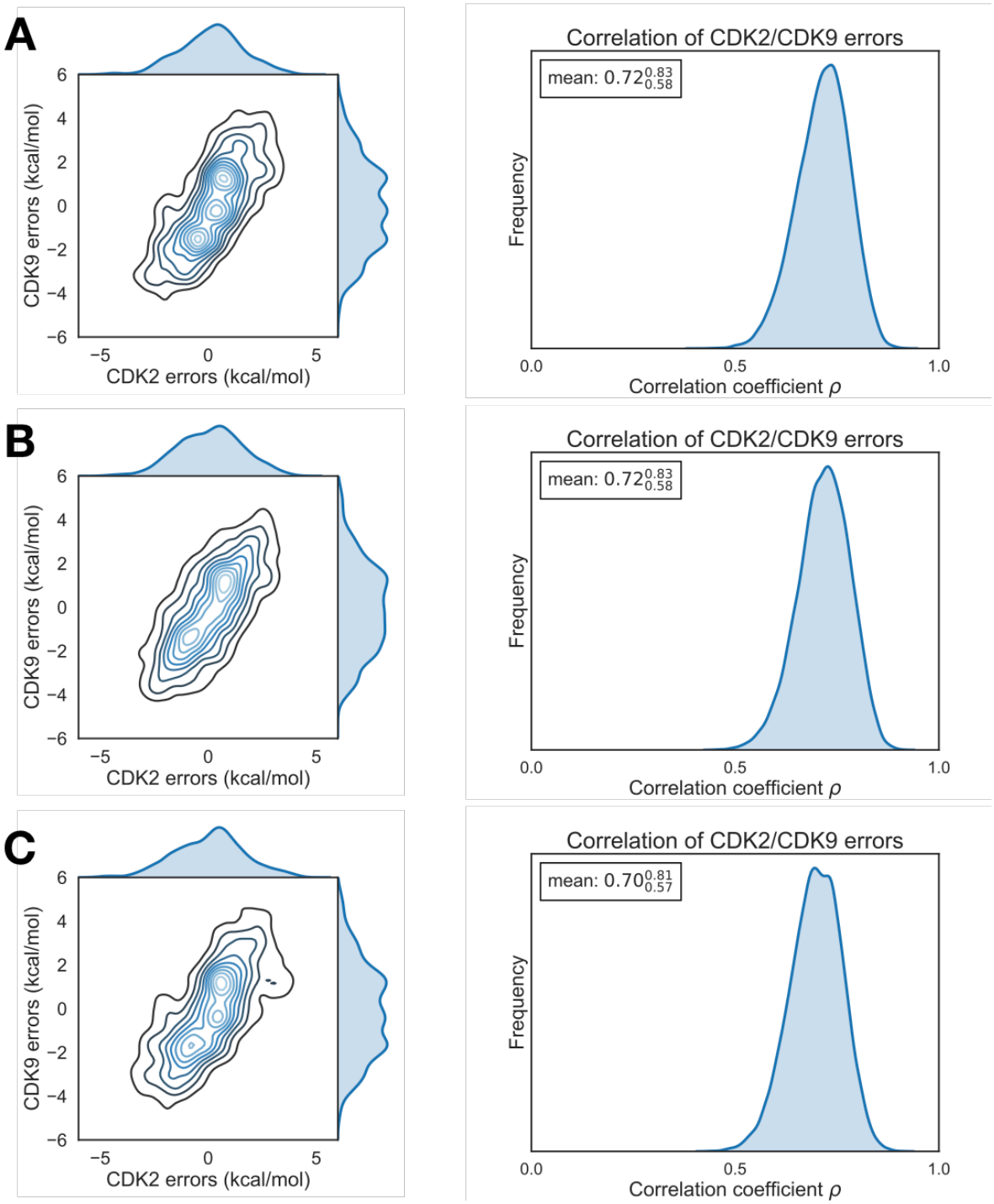

Supplemental Figure. 5. Each replicate of the CDK2/CDK9 calculations yields consistent errors and correlation coefficient

(**A**) (*left*) The joint posterior distribution of the prediction errors for CDK2 (X-axis) and CDK9 (Y-axis) from the Bayesian graphical model for replicate 1. (*right*) The posterior marginal distribution of the correlation coefficient (ρ) is shown in gray for replcicate 1. The inserted box shows the mean and 95% confidence interval for the correlation coefficient. (**B**) and (**C**) The same as above, but for replicates 2 and 3, respectively

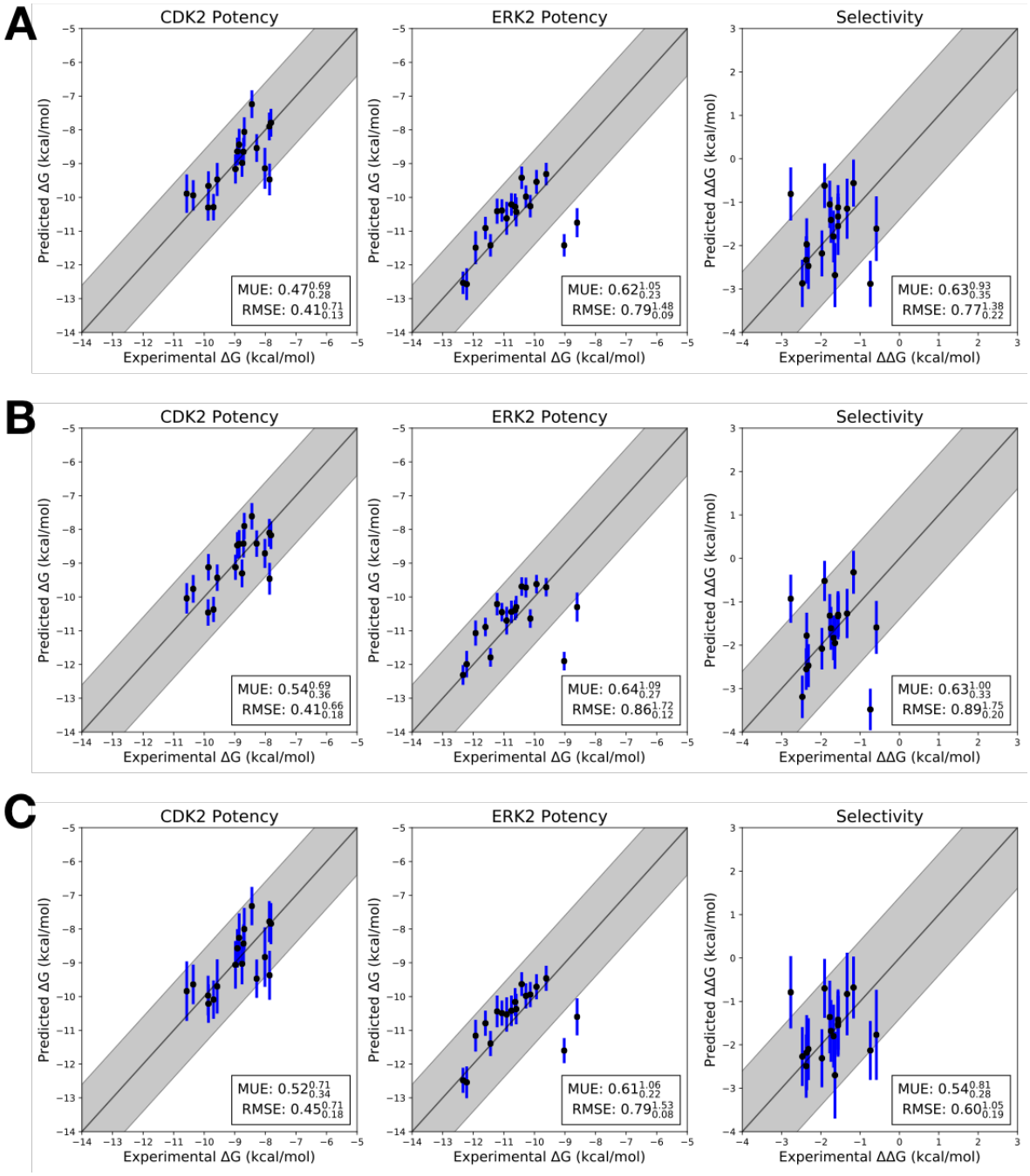

Supplemental Figure. 6. Each replicate of the CDK2/ERK2 calculations yields a consistent RMSE and MUE
hree replicates of the CDK2/ERK2 calculations with different random seeds, but otherwise the same input structures, files, and parameters. The experimental values are shown on the X-axis and calculated values on the Y-axis. Each data point corresponds to a ligand for a given target. All values are shown in units of kcal/mol. The horizontal error bars show the assumed experimental uncertainty of 0.3 kcal/mol[6].We show the 95% CI based on the estimated statistical as vertical blue error bars. For selectivity, the errors were propagated under the assumption that they were completely uncorrelated. The black line indicates agreement between calculation and experiment, while the gray shaded region represent 1.36 kcal/mol (or 1 log unit) error. The MUE and RMSE are shown on each plot with bootstrapped 95% confidence intervals. (**A**) Replicate 1 (**B**) Replicate 2 (**C**) Replicate 3

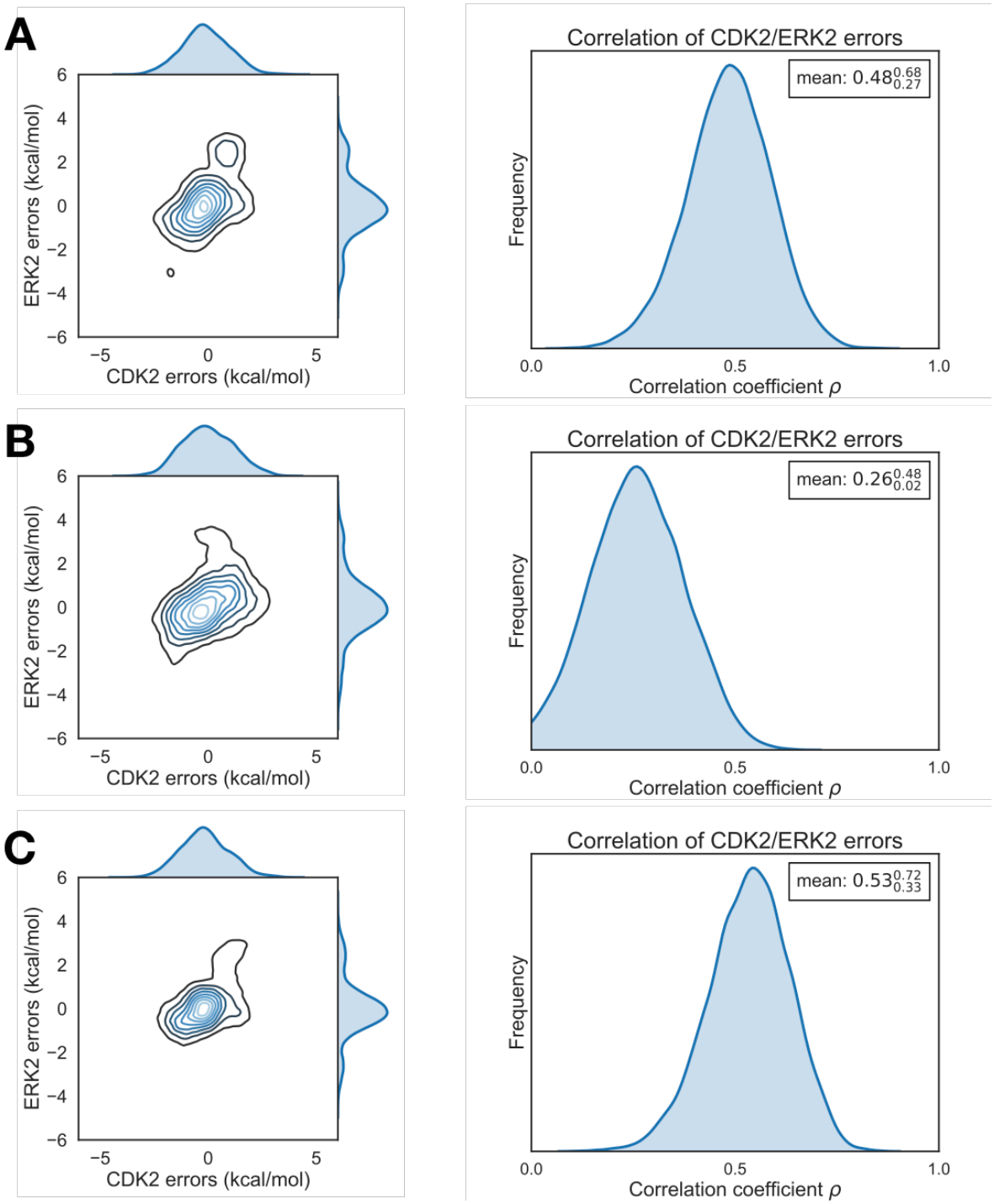

Supplemental Figure. 7. Each replicate of the CDK2/ERK2 calculations yields consistent errors and correlation coefficient

(**A**) (*left*) The joint posterior distribution of the prediction errors for CDK2 (X-axis) and ERK2 (Y-axis) from the Bayesian graphical model for replicate 1. (*right*) The posterior marginal distribution of the correlation coefficient (ρ) is shown in gray for replcicate 1. The inserted box shows the mean and 95% confidence interval for the correlation coefficient. (**B**) and (**C**) The same as above, but for replicates 2 and 3, respectively

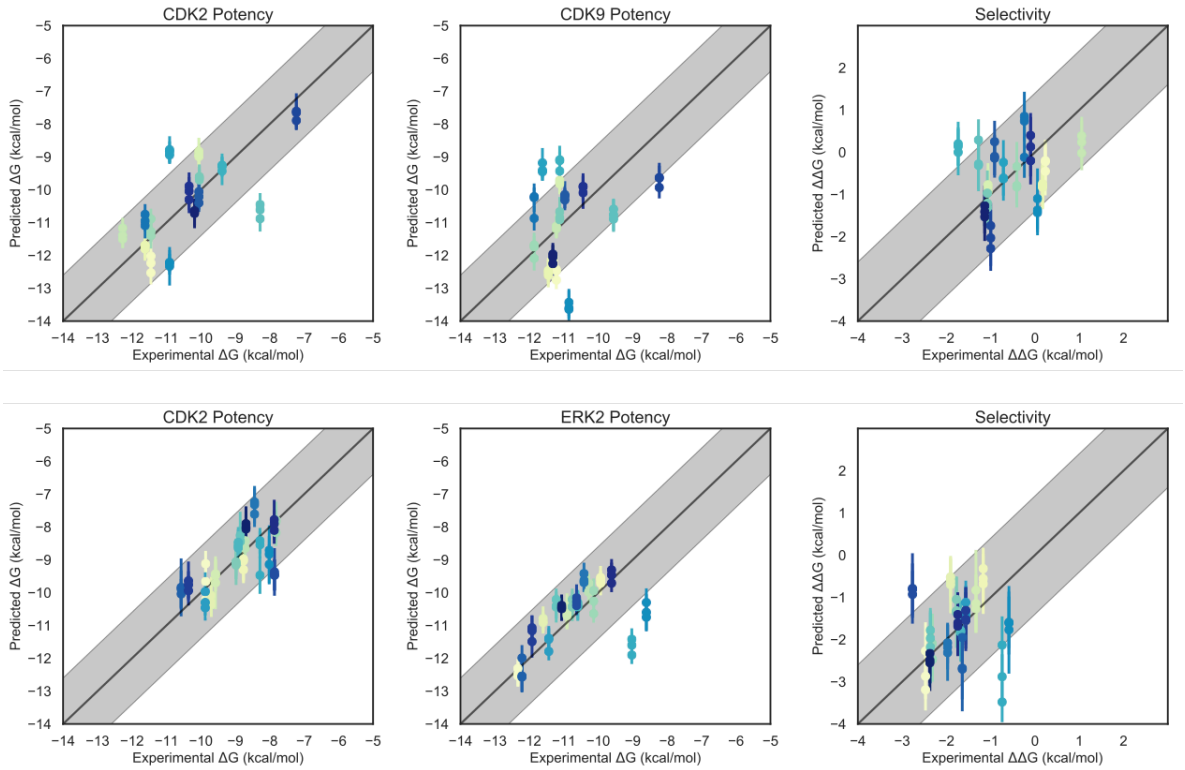

Supplemental Figure. 8. The pooled replicates show good agreement in predictions for individual ligands
The experimental values are shown on the X-axis and calculated values on the Y-axis. Each data point corresponds to a ligand for a given target. All values are shown in units of kcal/mol. The horizontal error bars show the assumed experimental uncertainty of 0.3 kcal/mol[6].We show the 95% CI based on the estimated statistical as vertical blue error bars. For selectivity, the errors were propagated under the assumption that they were completely uncorrelated. The black line indicates agreement between calculation and experiment, while the gray shaded region represent 1.36 kcal/mol (or 1 log unit) error. The MUE and RMSE are shown on each plot with bootstrapped 95% confidence intervals. (**Top**) CDK2/CDK9 replicates (**Bottom**) CDK2/ERK2 replicates

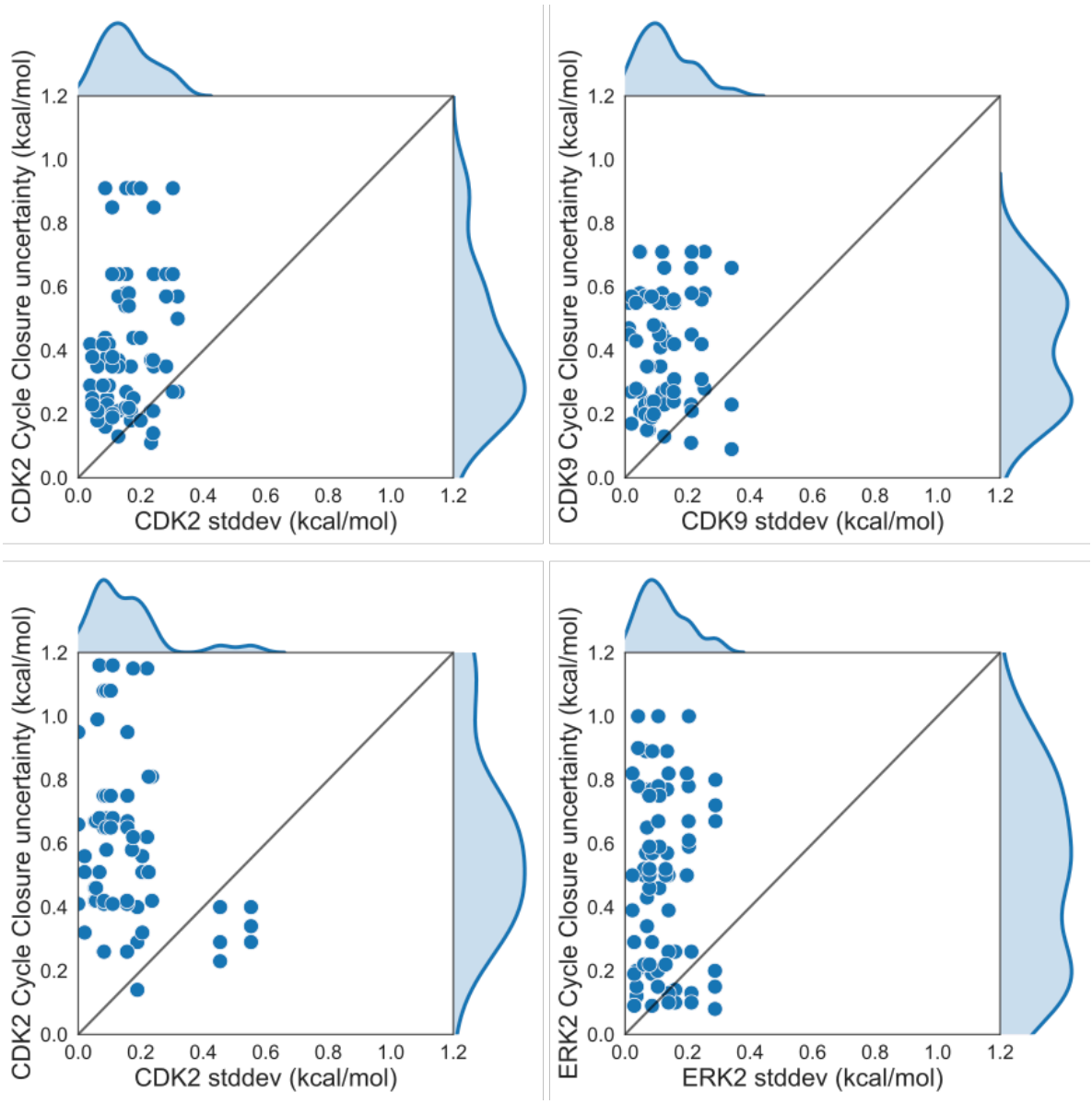

Supplemental Figure. 9. The standard deviation for each edge is smaller than the estimated cycle closure uncertainties

The cycle closure uncertainty for each edge of the map is shown on the Y-axis and the standard deviation for that edge in all three replicate calculations is shown on the X-axis, in kcal/mol. Each point corresponds to an edge of the FEP map. The edges for all three replicates are pooled and shown together. (**Top**) CDK2/CDK9 calculations (**Bottom**) CDK2/ERK2 calculations.